[American Journal of Science, Vol. 306, April, 2006, P. 246–294, DOI 10.2475/04.2006.02]

BIOENERGETIC CONTROLS ON ANAEROBIC OXIDATION OF METHANE (AOM) IN COASTAL MARINE SEDIMENTS: A THEORETICAL ANALYSIS

A. W. DALE*, P. REGNIER, and P. VAN CAPPELLEN

Department of Earth Sciences - Geochemistry, Utrecht University, Utrecht, Netherlands

ABSTRACT. A kinetic-bioenergetic reaction model for the anaerobic oxidation of methane (AOM) in coastal marine sediments is presented. The model considers a fixed depth interval of sediments below the zone of bioturbation (the window-of-observation), subject to seasonal variations of temperature and inputs of organic substrates and sulfate. It includes (1) nine microbially-mediated reaction pathways involved in CH_4 production/consumption; (2) an explicit representation of five functional microbial groups; and (3) bioenergetic limitations of the microbial metabolic pathways. Fermentation of organic substrates is assumed to produce hydrogen (H_2) and acetate (Ac) as key reactive intermediates. Competition among the metabolic pathways is controlled by the relative kinetic efficiencies of the various microbial processes and by bioenergetic constraints. Model results imply that the functional microbial biomasses within the window-of-observation undergo little variation over the year, as a result of kinetic and thermodynamic buffering of the seasonal forcings. Furthermore, the microbial processes proceed at only small fractions of their maximum potential rates. These findings provide a theoretical justification for the approximation of steady-state microbial biomasses, which is frequently used in diagenetic modeling. In contrast, AOM rates show a strong seasonal evolution: AOM only becomes spontaneous in winter, when hydrogenotrophic sulfate reduction (hySR) sufficiently reduces the local H_2 concentration. The bioenergetic limitation of AOM is thus a critical factor modulating this process in seasonally-forced nearshore marine sediments. A global sensitivity analysis based on a 2-level factorial design reveals that AOM rates are most sensitive to the kinetic parameters describing hySR and acetotrophic methanogenesis (acME). The growth and substrate uptake kinetics of AOM are unimportant, whereas the threshold value of ATP energy conservation for AOM is the most sensitive thermodynamic parameter. These results confirm that anaerobic methane oxidizing microorganisms are metabolizing close to their thermodynamic limit, with the energetic balance being controlled by the relative rates of hySR and acME. The removal of Ac by acME primarily allows more sulfate (SO_4^{2-}) to be utilized for H_2 oxidation, thereby promoting AOM.

INTRODUCTION

Methane (CH_4) is, after carbon dioxide (CO_2), the second most important greenhouse gas, accounting for 20 percent of the trapping of infrared radiation in the atmosphere (Mackenzie, 1998). Anoxic marine sediments constitute the largest methane reservoir on Earth, equivalent to perhaps 3 times the entire terrestrial biomass (Kvenvolden and others, 1993). Fluxes of CH_4 to the atmosphere from marine sediments therefore represent a key forcing of the climate system (Dickens and others, 1995; Dickens, 2003). Strikingly, however, around 90 percent of methane produced in marine sediments is consumed before reaching the seafloor, by a process known as the anaerobic oxidation of methane (Iversen, 1996; Reeburgh, 1996). Anaerobic oxidation of methane (AOM) is thus a process of global significance, yet our quantitative understanding of the controls on CH_4 fluxes and AOM rates in marine sediments remains very fragmentary. This limits our ability to predict the response to environmental perturbations of CH_4 release from the seafloor.

*Corresponding author: e-mail: dale@geo.uu.nl

AOM in marine sediments is the process by which CH_4 diffusing upwards through the anoxic sediment disappears before it can contact oxygen (Barnes and Goldberg, 1976; Reeburgh, 1976; Alperin and Reeburgh, 1985). It is generally accepted that AOM is coupled to sulfate (SO_4^{2-}) as the terminal electron acceptor (Hoehler and others, 1994; Boetius and others, 2000), typically within a restricted sediment depth interval of enhanced microbial activity known as the sulfate-methane transition zone (SMTZ). Mounting evidence supports a syntrophic association of methane-oxidizing archaea (MOA) and sulfate reducing bacteria (SRB) carrying out the following reactions (Hoehler and others, 1994; Hinrichs and others, 1999; Boetius and others, 2000; Orphan and others, 2002):

$$\text{MOA: } CH_{4(g)} + 3H_2O \rightarrow 4H_{2(g)} + HCO_3^-{}_{(aq)} + H^+{}_{(aq)} \qquad \Delta G^{o'} = 135.4 \text{ kJ (mol reaction)}^{-1} \quad (1)$$

$$\text{SRB: } SO_4^{2-}{}_{(aq)} + 4H_{2(g)} + H^+{}_{(aq)} \rightarrow HS^-{}_{(aq)} + 4H_2O \qquad \Delta G^{o'} = -152.3 \text{ kJ (mol reaction)}^{-1} \quad (2)$$

$$\text{Net: } CH_{4(g)} + SO_4^{2-}{}_{(aq)} \rightarrow HS^-{}_{(aq)} + H_2O + HCO_3^-{}_{(aq)} \qquad \Delta G^{o'} = -16.9 \text{ kJ (mol reaction)}^{-1} \quad (3)$$

where the standard Gibbs energies of reaction ($\Delta G^{o'}$) listed are for conditions of pH 7.0, 298K and 1 bar. Hydrogen (H_2) is used as a representative electron shuttle for energy transfer between the microbes in the above equations, although other reactive intermediates have been suggested (Sørensen and others, 2001). In addition, recent reports of the existence of mono-specific methane-oxidizing cells, cocci and rods suggests that AOM may also be carried out by single microbial species rather than consortia (Santegoeds and others, 1999; Orphan and others, 2001; Knittel and others, 2003). In this study, we focus on methane oxidation resulting from the coupled activity of MOA and SRB, although the exact spatial arrangements of the microbial species carrying out the reactions and corresponding transport limitations are not considered.

Despite recent advances, the environmental and physiological controls of AOM remain poorly constrained (Hinrichs and Boetius, 2002). The net, standard-state Gibbs energy yield of AOM at neutral pH is on the order of -16.9 kJ (mol reaction)$^{-1}$, to be shared by the partners of the microbial consortium. The useful energy generated by AOM coupled to sulfate reduction is thus quite small, given that the minimum energy threshold for microbial growth is usually assumed to be on the order of 15 to 20 kJ (mol reaction)$^{-1}$ (Schink, 1997). For typical *in situ* activities of CH_4 and SO_4^{2-} in the SMTZ (Bian and others, 2001) the energy yield is only slightly higher. The sluggish rates of AOM observed in the field (Jørgensen and others, 2001) further indicate that the microbial communities carrying out AOM operate close to their thermodynamic limit. Accordingly, the concentrations of reactive intermediates, particularly H_2 (Hoehler and others, 1998), play a central role in determining whether AOM is thermodynamically viable or not and, hence, in controlling the competition of AOM with other energy-yielding microbial processes. In fact, the H_2 concentration behaves as a thermodynamic switch: only when H_2 levels in the SMTZ are maintained below a threshold concentration by the SRB are the MOA able to oxidize CH_4 (Hoehler and others, 1998).

A major outstanding challenge in the development of reactive-transport models for subsurface environments is the incorporation of realistic microbial reaction networks (Davis and others, 2004). However, modeling microbial dynamics is limited by our understanding of the interactions between functionally diverse groups of organisms. Earlier modeling studies of AOM in marine environments have generally

ignored the production and consumption of reactive intermediates, instead focussing on the net AOM reaction (eq 3). For instance, a widely used expression for the rate of AOM (R_{AOM}) in early diagenetic models assumes a bimolecular dependence on the CH_4 and SO_4^{2-} concentrations (Van Cappellen and Wang, 1996; Haese and others, 2003; Luff and Wallmann, 2003; Luff and others, 2004):

$$R_{AOM} = k_{AOM}[SO_4^{2-}][CH_4] \quad (4)$$

where k_{AOM} is an apparent second-order rate constant (concentration^{-1} time^{-1}). While simple rate equations, such as equation (4), are usually able to reproduce the distributions of reactants and rates of CH_4 turnover in the SMTZ, the resulting rate parameters (k_{AOM} in eq 4) are at best fitting parameters. In itself, equation (4) does not provide insight into possible thermodynamic limitation of AOM, the regulation of AOM rates by microbial growth and decay processes, or the role of intermediate energy substrates. Therefore, the predictive capability of equation (4) remains limited.

In sediments, direct energy substrates for SRB, for example H_2 and acetate, are generated through the fermentative degradation of organic compounds (Zehnder and Stumm, 1988). In particular, in non-seep coastal marine sediments, sulfate reduction (SR) coupled to methane oxidation directly competes with SR coupled to the oxidation of fermentation products. As the latter may also serve as substrates for methanogenesis, AOM forms an integral part of a complex network of coupled reaction pathways. A theoretical analysis of this reaction network and its consequences for AOM rates in coastal marine sediments is the goal of the present study.

To this end, we develop an open, batch-reactor model representative of anaerobic sediment from the SMTZ in a coastal marine setting subject to seasonal forcings in sulfate, organic matter supply and temperature. The model includes (1) a comprehensive reaction network comprising the production and consumption of CH_4, (2) explicit representations of the microbial biomasses, and (3) inclusion of the thermodynamic limitations of the microbial reaction pathways. Microbial biomasses are frequently represented explicitly in models used in bioengineering and groundwater applications (Rittmann and VanBriesen, 1996; Schäfer and others, 1998), yet this is rarely done in early diagenetic models (Talin and others, 2003). This reflects not only the increased model complexity and additional parameterizations needed to describe the microbial growth and decay, but also the implicit assumption that microbial communities in sediments are able to rapidly adjust their activity levels to changes in substrate availability (Van Cappellen and Gaillard, 1996). Using a biomass-explicit reaction model, we investigate the validity of this assumption for CH_4 production and consumption in coastal marine sediments.

MODELING STRATEGY

Model Concept and Forcing Functions

The model simulates temporal changes within a fixed depth interval below the sediment-water interface, in a shallow water (20 m), temperate climate, marine depositional setting (fig. 1). The selected depth interval, or "window-of-observation", is located below the zone of bioturbation in the permanently anaerobic portion of the sediment. It experiences seasonal fluctuations of temperature and influxes of labile organic carbon substrates plus SO_4^{2-} (fig. 1) which are assumed to be completely utilized within the given depth interval. In particular, because of pronounced seasonal variations in sediment metabolism (see Klump and Martens, 1989; Alperin and others, 1994; Koretsky and others, 2005; Treude and others, 2005), the SO_4^{2-} penetration depth is assumed to be shallower than the upper boundary of the selected depth interval during the summer, and vice versa during winter. Thus, over a yearly cycle, the

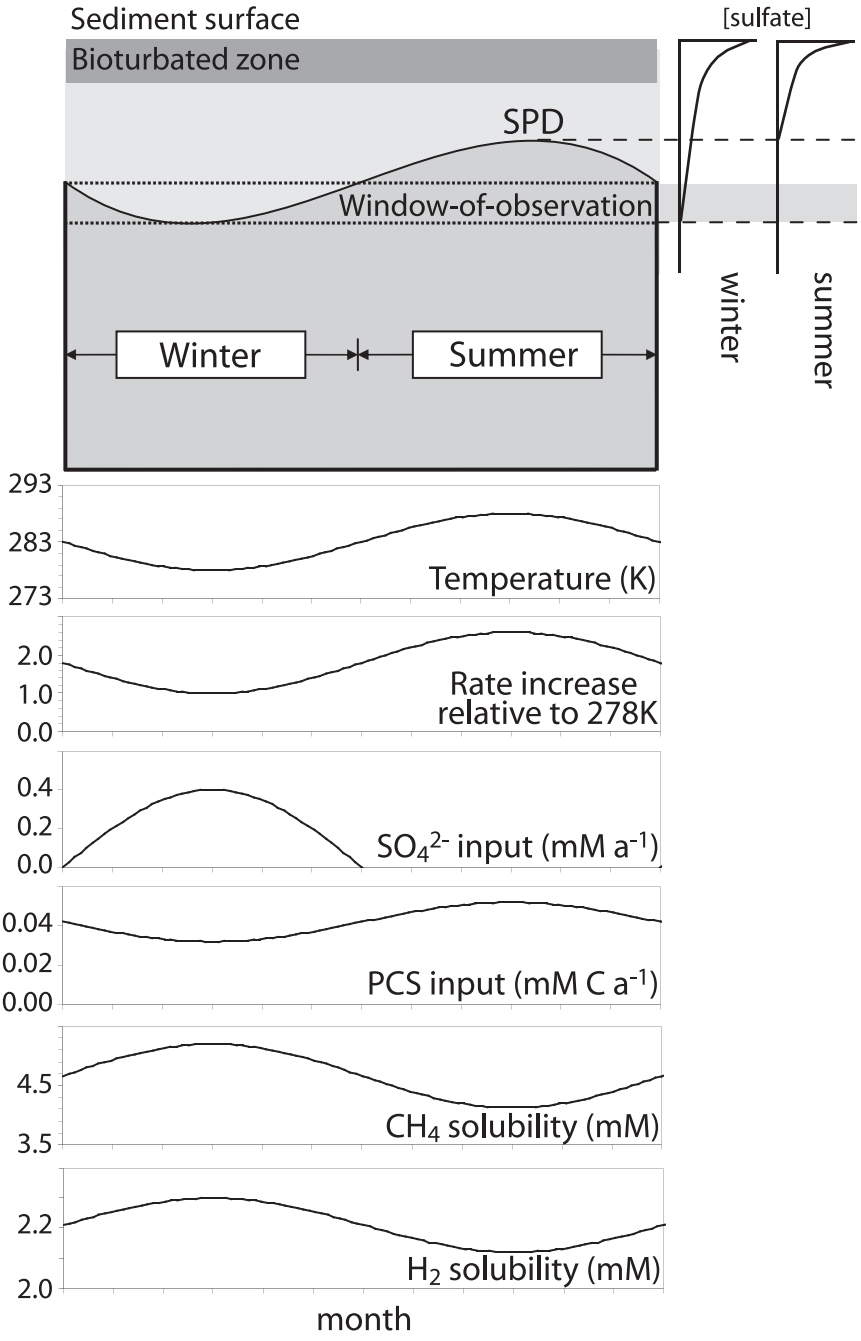

Fig. 1. Model concept and forcings. The top schematic shows how the sulfate penetration depth (SPD) varies seasonally relative to the fixed window-of-observation. The SPD is deeper in winter than in summer due to lower temperature and organic matter supply. Corresponding down-core sulfate profiles are shown at the top right. The lower panels show the seasonal forcings imposed on the window-of-observation. See text for detailed discussion.

early diagenetic regime within the window-of-observation is expected to shift from being dominated by SR (winter) to being dominated by methanogenesis (summer).

Pressure (3 bar) and salinity (35.5 ‰) are assumed to remain constant, while temperature varies sinusoidally from a minimum of 278K in winter to a maximum of 288K in summer (fig. 1). The supply flux of labile organic substrates peaks during the summer, with a maximum influx of primary carbon substrates (PCS) of 0.14 nmol cm^{-3} d^{-1} (fig. 1). The terminal electron acceptor, SO_4^{2-}, is only supplied to the selected depth interval during the 6 winter months (fig. 1). The yearly SO_4^{2-} input equals 127 μM, which is ~3 higher than the yearly PCS input (45 μM). The relative influxes of SO_4^{2-} and PCS are adjusted so that the maximum SO_4^{2-} concentrations in the window-of-observation are maintained within the range 50 to 100 μM (Iversen and Blackburn, 1981; Devol and others, 1984; Alperin and Reeburgh, 1985; Iversen and Jørgensen, 1985; Hansen and others, 1998; Martens and others, 1998). At these concentrations, characteristic of the base of the SMTZ, seasonal competition for reactive intermediates can occur, and year-round competitive inhibition by sulfate reducing bacteria over other biomass species (a situation prevailing in the permanently sulfate-reducing sediment layer above the window-of-observation) is avoided. Importantly, simultaneously increasing or decreasing the influxes of SO_4^{2-} and PCS, while keeping their relative magnitudes constant, do not affect the main conclusions of the study (results not shown).

Low molecular weight organic compounds (that is, PCS) are produced primarily by the extracellular enzymatic hydrolysis of high molecular weight organic detritus (Brüchert and Arnosti, 2003). For simplicity, PCS are treated here as consisting of glucose ($C_6H_{12}O_6$), in order to facilitate mass balance and Gibbs energy calculations. Fermentation of PCS produces reactive intermediate species that can be taken up by the cells, most importantly hydrogen (H_2) and acetate (Ac). H_2 is a major electron donor for many genera of bacteria and methanogenic archaea (Lovley and Klug, 1986; Schink, 1997), while Ac is the most abundant volatile fatty acid in nearshore marine systems (Winfrey and Ward, 1983; Brüchert and Arnosti, 2003), and a key intermediate for methanogenesis (Widdel, 1988).

CH_4 and H_2 are modeled as dissolved species, although partial pressures are used in the thermodynamic calculations. Partial pressures are calculated as a function of the temperature-dependent algorithms of Crozier and Yamamoto (1974) and Yamamoto and others (1976). As HCO_3^- and HS^- are not included as independent variables in the reaction network model, constant concentrations, $[HCO_3^-]$ = 10 mM and $[HS^-]$ = 1.5 mM, are imposed in Gibbs energy calculations. Sensitivity analyses (not shown) indicate that variations in $[HCO_3^-]$ and $[HS^-]$, within reasonable expected ranges, play a relatively minor role in the kinetic and thermodynamic regulation of AOM.

Activation energies reported for methanogens (70 – 140 kJ mol^{-1}, Schulz and Conrad, 1996) and sulfate reducers (36 – 132 kJ mol^{-1}, Westrich and Berner, 1988) are consistent with a strong temperature dependence of the activities of microorganisms in anoxic marine environments (Crill and Martens, 1987; Knoblauch and Jorgensen, 1999; Knoblauch and others, 1999; Kotsyurbenko and others, 2001; Avery and others, 2002; Koretsky and others, 2003; Weston and Joye, 2005). In the model calculations, rates vary according to the Arrhenius expression (Westrich and Berner, 1984), using a constant Q_{10} of 2.6 to account for the effects of the seasonal temperature variations on all microbial growth rates (fig. 1). A list of abbreviations and acronyms used throughout this paper is presented in table 1.

Microbial Biomasses and Catabolism

The microbial reaction network of the model is based on combinations of half-reactions between electron donors (E_D) and electron acceptors (E_A). The result-

TABLE 1

Glossary of terms used throughout the text

Term	Description
acME	Acetotrophic methanogenesis
acSR	Acetotrophic sulfate reduction
ACB	Acetogenic bacteria
AOM	Anaerobic oxidation of methane
B_i	Biomass of microbial group *i* (SRB, MET, MOA, ACB, FER)
E_A	Electron acceptor
E_D	Electron donor
fe	Fraction of electron-donor equivalents invested in catabolism
fs	Fraction of electron-donor equivalents invested in anabolism
FER	Fermenting bacteria
F_K	Kinetic driving force
F_T	Thermodynamic driving force
hyME	Hydrogenotrophic methanogenesis
hySR	Hydrogenotrophic sulfate reduction
K_S	Half-saturation constant
$m\Delta G_{ATP}$	Gibbs energy threshold for ATP production
MET	Methanogenic archaea
MOA	Methane-oxidizing archaea
PCS	Primary carbon substrates
Q_{10}	Relative rate increase per 10°C increase in temperature
SMTZ	Sulfate-methane transition zone
SR	Sulfate reduction
SRB	Sulfate reducing bacteria
Y	Microbial growth yield
ΔG_{NET}	Surplus Gibbs energy available for growth
ΔG_r	Gibbs energy of reaction under non-standard conditions
$\Delta G^{o\prime}$	Standard Gibbs energy of reaction at neutral pH
χ	Average stoichiometric number (ASN)
μ	Maximum specific growth rate
μ_e	Maximum specific endogenous decay rate

ing overall reactions generate useful energy for the organisms. Table 2 identifies the half-reactions (R_1-R_6), and their stoichiometric combinations into catabolic reactions (R_7-R_{15}). The reaction network is depicted schematically in figure 2: it includes sulfate reduction (R_7-R_8), methanogenesis (R_9-R_{10}), anaerobic methane oxidation (R_{11}-R_{12}), acetogenesis (R_{13}), acetotrophy (R_{14}) and fermentation (R_{15}). These reactions are mediated by 5 functional groups of microbes: fermenters (FER), sulfate reducing bacteria (SRB), methane oxidizing archaea (MOA), methanogens (MET) and homoacetogens (ACB). We assume that SRB are not able to metabolize PCS (Widdel, 1988; Chidthaisong and Conrad, 2000; Ingvorsen and others, 2003), hence, only FER are able to utilize PCS directly. The spatial arrangements of biomasses and, consequently, diffusion of reactive intermediates between cells, are not explicitly represented in the model (Dolfing, 1992; Sørensen and others, 2001).

TABLE 2

Redox half-reactions (R_1-R_6) and microbial redox processes (R_7-R_{15}). Gibbs energy changes are expressed on an electron equivalent basis (kJ e-eq^{-1}). Reactions R_7 to R_{15} are mediated by 5 separate microbial groups abbreviated in parentheses (see table 1). $\Delta G^{o'}$ refers to standard Gibbs energies corrected for biologically neutral pH conditions (298K and 1 bar) with the transformation $\Delta G^{o'} = \Delta G^{0} - Rtv_{H^+} ln[Kw^{0.5}]$, where v_{H^+} is the stoichiometric coefficient of H^+ in the reaction (Amend and Shock, 2001) and Kw is the ion product. $\Delta G'_r$ values correspond to a typical in situ pore water composition of coastal marine sediments (see footnote).

	Half-reactions	ΔG^o (298K)
R_1	$H^+_{(aq)} + e^- = {}^1/_2\, H_{2(g)}$	+39.95
R_2	${}^1/_8\, SO_4^{2-}{}_{(aq)} + {}^9/_8\, H^+_{(aq)} + e^- = {}^1/_8\, HS^-_{(aq)} + {}^1/_2\, H_2O$	+20.91
R_3	${}^1/_8\, HCO_3^-{}_{(aq)} + {}^9/_8\, H^+_{(aq)} + e^- = {}^1/_8\, CH_{4(g)} + {}^3/_8\, H_2O$	+23.03
R_4	${}^1/_4\, HCO_3^-{}_{(aq)} + {}^9/_8\, H^+_{(aq)} + e^- = {}^1/_8\, CH_3COO^-_{(aq)} + {}^1/_2\, H_2O$	+26.90
R_5	${}^1/_{20}\, NH_4^+{}_{(aq)} + {}^1/_4\, HCO_3^-{}_{(aq)} + {}^6/_5\, H^+_{(aq)} + e^- = {}^1/_{20}\, C_5H_7O_2N_{(s)} + {}^{13}/_{20}\, H_2O$	-15.52
R_6	${}^1/_4\, HCO_3^-{}_{(aq)} + {}^5/_4\, H^+_{(aq)} + e^- = {}^1/_{24}\, C_6H_{12}O_{6(aq)} + {}^1/_2\, H_2O$	+16.43

	Microbial redox reactions			$\Delta G^{o\prime}$ (298K)	$\Delta G'^{\dagger}_r$ (283K)
	Type	Formula	Stoichiometry		
R_7	Sulfate reduction (SRB)	R_2-R_1	${}^1/_2\, H_2 + {}^1/_8\, SO_4^{2-} + {}^1/_8\, H^+ \rightarrow {}^1/_8\, HS^- + {}^1/_2\, H_2O$	-19.04	-2.72
R_8	Sulfate reduction (SRB)	R_2-R_4	${}^1/_8\, CH_3COO^- + {}^1/_8\, SO_4^{2-} \rightarrow {}^1/_8\, HS^- + {}^1/_4\, HCO_3^-$	-6.00	-5.12
R_9	Methanogenesis (MET)	R_3-R_1	${}^1/_2\, H_2 + {}^1/_8\, HCO_3^- + {}^1/_8\, H^+ \rightarrow {}^1/_8\, CH_4 + {}^3/_8\, H_2O$	-16.92	+1.18
R_{10}	Methanogenesis (MET)	R_3-R_4	${}^1/_8\, CH_3COO^- + {}^1/_8\, H_2O \rightarrow {}^1/_8\, CH_4 + {}^1/_8\, HCO_3^-$	-3.88	-1.37
R_{11}	Methane oxidation (MOA)	R_1-R_3	${}^1/_8\, CH_4 + {}^3/_8\, H_2O \rightarrow {}^1/_2\, H_2 + {}^1/_8\, HCO_3^- + {}^1/_8\, H^+$	+16.92	-1.18
R_{12}	Methane oxidation (MOA)	R_4-R_3	${}^1/_8\, CH_4 + {}^1/_8\, HCO_3^- \rightarrow {}^1/_8\, CH_3COO^- + {}^1/_8\, H_2O$	+3.88	+1.37
R_{13}	Acetogenesis (ACB)	R_4-R_1	${}^1/_2\, H_2 + {}^1/_4\, HCO_3^- + {}^1/_8\, H^+ \rightarrow {}^1/_8\, CH_3COO^- + {}^1/_2\, H_2O$	-13.05	+2.55
R_{14}	Acetotrophy (ACB)	R_1-R_4	${}^1/_8\, CH_3COO^- + {}^1/_2\, H_2O \rightarrow {}^1/_2\, H_2 + {}^1/_4\, HCO_3^- + {}^1/_8\, H^+$	+13.05	-2.55
R_{15}	Fermentation (FER)	$2R_4$+R_1-$3R_6$	${}^1/_8\, C_6H_{12}O_6 + {}^1/_2\, H_2O \rightarrow {}^1/_4\, CH_3COO^- + {}^1/_2\, H_2 + {}^1/_2\, H^+ + {}^1/_4\, HCO_3^-$	-25.84	-50.48

†Typical coastal marine conditions (283 K), $\{CH_4\}$ = 1 atm; $\{H_2\}$ = 0.5 μatm; [Ac] = 2×10^{-6} M; γ_{Ac} = 0.68; $[SO_4^{2-}]$ = 0.02 M; γ_{SO4} = 0.10; $[HS^-]$ = 1.5×10^{-3} M; γ_{HS} = 0.53; $[HCO_3^-]$ = 0.01 M; γ_{HCO3} = 0.53; $[C_6H_{12}O_6]$ = 1×10^{-3} M; $\gamma_{C6H12O6}$ = 1.17, where γ_j is the activity coefficient of species j (Morel and Herring, 1993; Millero and Pierrot, 1998).

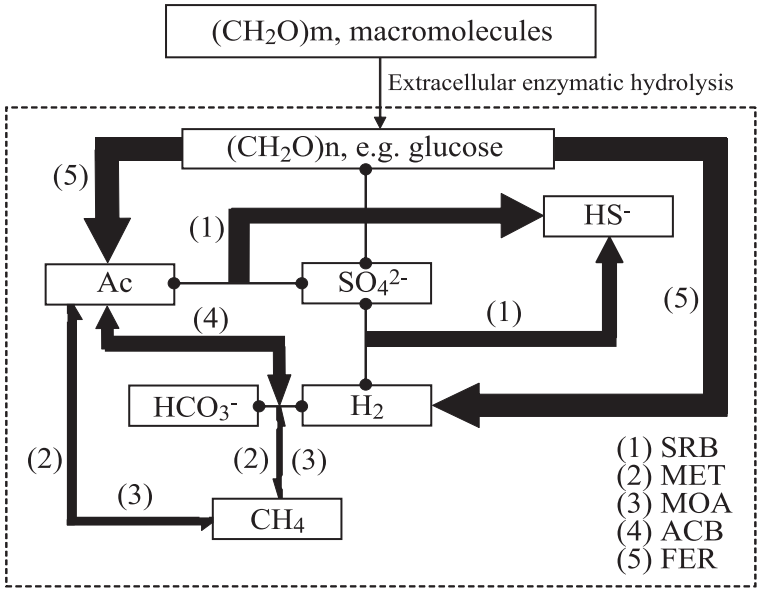

Fig. 2. Schematic representation of the model reaction network (within dashed box). The supply fluxes of primary carbon substrate (PCS) and sulfate (SO_4^{2-}) are external forcings in the model (fig. 1). Here PCS is represented as glucose. The 9 modeled pathways are mediated by the microbial species indicated. The relative arrow thicknesses correspond to the Gibbs energy released under *in situ* conditions (see table 2). Key: SRB, sulfate reducing bacteria; MET, methanogenic archaea; MOA, methane oxidizing archaea; ACB, homoacetogenic bacteria; FER, fermenting bacteria.

The selected catabolic and anabolic pathways of the reaction network are those associated with the microorganisms most commonly reported in AOM environments. The prominent SRB species are the Gram-negative bacteria *Desulfosarcina* and *Desulfococcus* spp. of the δ-proteobacteria (Boetius and others, 2000; Michaelis and others, 2002; Orphan and others, 2002). MOA species have been phylogenetically identified as one of several groups of methanotrophic archaea (for example, ANME 1, ANME 2; Hinrichs and Boetius, 2002), while the methanogens (MET) are assumed to belong to the *Methanosarcina* genera using H_2 or Ac as electron donor (Whitman and others, 2004). A close resemblance between MOA and *Methanosarcina* is suggested by FISH (Orphan and others, 2002) and biomarker evidence (Pancost and others, 2000; Bian and others, 2001). Moreover, recent discoveries of a novel nickel protein in AOM archaea from Black Sea methane seeps suggests a reversed mechanism of CH_4 metabolism (Krüger and others, 2003). Therefore, in the model, MOA are considered to metabolize in one direction only (irreversible metabolism), using H_2O or HCO_3^- as electron acceptor (R_{11}-R_{12}, table 2). New genomic evidence of MOA also suggests that oxidation to hydrogen is a feasible pathway of methane oxidation (Hallam and others, 2004), despite other inconclusive experimental evidence (Nauhaus and others, 2002). Little is known about acetogenic (ACB) bacteria in the SMTZ. The ACB are assumed to be functionally similar to the acetate oxidizing rod or "*Reversibacter*" (Zinder and Koch, 1984; Lee and Zinder, 1988; Schink, 1997), capable of both acetetogenesis (R_{13}) and acetotrophy (R_{14}). The latter occurs when H_2 becomes sufficiently depleted, which is a characteristic feature of the SMTZ (Hoehler and others, 1994). Fermentation of PCS (R_{15}) is only included in order to produce reduced reactive intermediates that serve as direct energy substrates, and as such the fermenting organisms are unspecified.

In this work, we use well-established conventions to describe catabolic and anabolic pathways (Brock and others, 1994). Biomass synthesis (R_5) assumes a biomass composition of $C_5H_7O_2N$ (Rittman and McCarty, 2001). As detailed in the next section, cellular synthesis is coupled to the catabolic reactions R_7-R_{15}, to form the macrochemical equations implemented in the reaction network. Coupled reactions R_8, R_{10}, R_{14}, R_{15} (table 2) use organic substrates as electron donor and carbon source, and thus represent heterotrophic pathways. The methane oxidizing reactions (R_{11}, R_{12}) are also assumed to be heterotrophic. In contrast, reactions using H_2 as energy source (R_7, R_9, R_{13}) exemplify autotrophic growth and require an inorganic carbon source. This is in accord with known metabolic pathways of *Desulfosarcina*, *Methanosarcina* and *Reversibacter* (Simpson and Whitman, 1993; Drake, 1994; Zinder, 1994; Rabus and others, 2004; Whitman and others, 2004).

Coupled Bioenergetic-Kinetic Microbial Growth Model

The core of the mathematical model is a set of differential equations describing microbial growth and substrate utilization kinetics, coupled to thermodynamic limitation. Competition among terminal electron accepting processes is not regulated by *ad hoc* inhibition terms, but rather derives from the relative rates of the various pathways in the reaction network (Watson and others, 2003; Thullner and others, 2005). The macrochemical equations (table 3) are created by combining catabolic and anabolic reactions and, thus, describe gross synthesis of biomass through the utilization of an electron donor (E_D), an electron acceptor (E_A) and a carbon source (Heijnen and others, 1993). To formulate these equations, we closely follow the systematic approach of Rittmann and McCarty (2001) and VanBriesen (2002). The Appendices provide the detailed theoretical background for the derivation of the microbial growth parameters.

Electrons supplied by an E_D are used partially to generate energy and partially for biomass synthesis (see Appendix 1). The fractions of electrons used for energy and biomass production are termed *fe* and *fs*, respectively. The latter fraction is equivalent to the cell growth yield on an electron-equivalent basis. Details on how *fs* is related to the more common yield term, *Y*, are given in Appendix 1. If the stoichiometries of the reduction half-reactions of the E_D, E_A and biomass synthesis are Rd, Ra and Rc, respectively, the stoichiometry of the macrochemical equation for growth, Rm, is given by (Rittmann and McCarty, 2001):

$$\mathrm{Rm} = fe\,(\mathrm{Ra} - \mathrm{Rd}) + fs\,(\mathrm{Rc} - \mathrm{Rd}) \tag{5}$$

which expresses the partitioning of electrons from the E_D into catabolism and cell synthesis. Since $fe+fs$ must be equal to 1, rearrangement of equation (5) leads to the following expression for cell synthesis:

$$\mathrm{Rm} = fe\,\mathrm{Ra} + fs\,\mathrm{Rc} - \mathrm{Rd} \tag{6}$$

The reduction half-reactions are listed as R_1-R_6 in table 2, where R_5 is the half-reaction for biomass ($C_5H_7O_2N$) synthesis. Values of *fs*, derived according to the method presented in Appendix 1, are given in table 4. Values of *fe* are then obtained as $fe = 1 - fs$. Table 3 presents the macrochemical equations (R_{7m}-R_{15m}) and reaction stoichiometries corresponding to the catabolic reactions (R_7-R_{15}) of table 2. Note that each macrochemical formula reaction yields one mole C of biomass. The reaction stoichiometries couple the changes in concentrations of all the reactive chemical and biological species in the model.

Using hydrogenotrophic sulfate reduction (R_7, table 2) as an example, the stoichiometry of the macrochemical equation R_{7m} (table 3) is:

TABLE 3

Macrochemical equations and stoichiometries of the reaction network. In each case, 1 C-mol biomass ($C_5H_7O_2N$) is synthesized

	Macrochemical equation	Stoichiometry
R_{7m}	$fe^{H2}_{SRB}R_2 + fs^{H2}_{SRB}R_5 - R_1$	$(fe/2fs)SO_4^{2-} + 0.2NH_4^+ + ((5+3fs)/10fs)H^+ + HCO_3^- + (2/fs)H_2 \rightarrow 0.2C_5H_7O_2N + (fe/2fs)HS^- + ((10+3fs)/5fs)H_2O$
R_{8m}	$fe^{Ac}_{SRB}R_2 + fs^{Ac}_{SRB}R_5 - R_4$	$(fe/2fs)SO_4^{2-} + 0.3H^+ + 0.2NH_4^+ + (1/2fs)CH_3COO^- \rightarrow 0.2C_5H_7O_2N + (fe/2fs)HS^- + (fe/fs)HCO_3^- + 0.6H_2O$
R_{9m}	$fe^{H2}_{MET}R_3 + fs^{H2}_{MET}R_5 - R_1$	$((1+fs)/2fs))HCO_3^- + 0.2NH_4^+ + ((5+fs)/10fs))H^+ + (2/fs)H_2 \rightarrow 0.2C_5H_7O_2N + (fe/2fs)CH_4 + ((15+11fs)/10fs))H_2O$
R_{10m}	$fe^{Ac}_{MET}R_3 + fs^{Ac}_{MET}R_5 - R_4$	$(1/2fs)CH_3COO^- + 0.2NH_4^+ + ((5\text{-}11fs)/10fs)H_2O + 0.3H^+ \rightarrow 0.2C_5H_7O_2N + (fe/2fs)CH_4 + (fe/2fs)HCO_3^-$
R_{11m}	$fe^{CH4H2O}_{MOA}R_1 + fs^{CH4H2O}_{MOA}R_5 - R_3$	$(1/2fs)CH_4 + 0.2NH_4^+ + ((15\text{-}26fs)/10fs)H_2O \rightarrow 0.2C_5H_7O_2N + ((5\text{-}8fs)/10fs)H^+ + (2fe/fs)H_2 + ((1\text{-}2fs)/2fs)HCO_3^-$
R_{12m}	$fe^{CH4CO2}_{MOA}R_4 + fs^{CH4CO2}_{MOA}R_5 - R_3$	$(1/2fs)CH_4 + 0.2NH_4^+ + 0.3H^+ + (1/2fs)HCO_3^- \rightarrow 0.2C_5H_7O_2N + (fe/2fs)CH_3COO^- + ((5+6fs)/10fs)H_2O$
R_{13m}	$fe^{H2}_{ACB}R_4 + fs^{H2}_{ACB}R_5 - R_1$	$(2/fs)H_2 + 0.2NH_4^+ + (1/fs)HCO_3^- + ((5+3fs)/10fs)H^+ \rightarrow 0.2C_5H_7O_2N + (fe/2fs)CH_3COO^- + ((10+3fs)/5fs)H_2O$
R_{14m}	$fe^{Ac}_{ACB}R_1 + fs^{Ac}_{ACB}R_5 - R_4$	$(1/2fs)CH_3COO^- + 0.2NH_4^+ + ((10\text{-}13fs)/5fs)H_2O \rightarrow 0.2C_5H_7O_2N + (2fe/fs)H_2 + (fe/fs)HCO_3^- + ((5\text{-}8fs)/10fs)H^+$
R_{15m}	$fe^{PCS}_{FER}(\frac{2}{3}R_4 + \frac{1}{3}R_1) + fs^{PCS}_{FER}R_5 - R_6$	$(1/6fs)C_6H_{12}O_6 + 0.2NH_4^+ + ((10\text{-}19fs)/15fs))H_2O \rightarrow$ $0.2C_5H_7O_2N + (fe/3fs)CH_3COO^- + (2fe/3fs)H_2 + (fe/3fs)HCO_3^- + ((10\text{-}7fs)/15fs)H^+$

TABLE 4

Growth-related parameters used in the baseline simulation and corresponding sensitivity ranges tested. Maximum specific growth and decay rates listed are values at 278K. (ASN = average stoichiometric number)

Parameter	Description	Baseline value	Units	Footnote ref.	Sensitivity
K_{S-SRB}^{SO4}	Half-saturation constant of SO_4^{2-} for SRB	1×10^{-3}	mol L^{-1}	1	±25%
K_{S-SRB}^{H2}	Half-saturation constant of H_2 for SRB	1×10^{-8}	mol L^{-1}	2	±25%
K_{S-SRB}^{Ac}	Half-saturation constant of Ac for SRB	1×10^{-4}	mol L^{-1}	3	±25%
K_{S-MET}^{H2}	Half-saturation constant of H_2 for MET	1×10^{-6}	mol L^{-1}	4	±25%
K_{S-MET}^{Ac}	Half-saturation constant of Ac for MET	1×10^{-3}	mol L^{-1}	5	±25%
K_{S-MOA}^{CH4}	Half-saturation constant of CH_4 for MOA	1.5×10^{-3}	mol L^{-1}	6	±25%
K_{S-ACB}^{H2}	Half-saturation constant of H_2 for ACB	1×10^{-7}	mol L^{-1}	7	±25%
K_{S-ACB}^{Ac}	Half-saturation constant of Ac for ACB	1×10^{-3}	mol L^{-1}	8	±25%
K_{S-FER}^{PCS}	Half-saturation constant of PCS for FER	1×10^{-3}	mol L^{-1}	9	-
fs_{SRB}^{H2}	Cell yield of SRB growing on H_2	0.049	e-eq cells (e-eq H_2)$^{-1}$	Calculated	±25%
fs_{SRB}^{Ac}	Cell yield of SRB growing on Ac	0.074	e-eq cells (e-eq Ac)$^{-1}$	Calculated	±25%
fs_{MET}^{H2}	Cell yield of MET growing on H_2	0.044	e-eq cells (e-eq H_2)$^{-1}$	Calculated	±25%
fs_{MET}^{Ac}	Cell yield of MET growing on Ac	0.049	e-eq cells (e-eq Ac)$^{-1}$	Calculated	±25%
fs_{MOA}^{CH4H2O}	Cell yield of MOA growing on CH_4+H_2O	0.035	e-eq cells (e-eq CH_4)$^{-1}$	Assumed	±25%
fs_{MOA}^{CH4CO2}	Cell yield of MOA growing on CH_4+CO_2	0.035	e-eq cells (e-eq CH_4)$^{-1}$	Assumed	±25%
fs_{ACB}^{H2}	Cell yield of ACB growing on H_2	0.034	e-eq cells (e-eq H_2)$^{-1}$	Calculated	±25%
fs_{ACB}^{Ac}	Cell yield of ACB growing on Ac	0.035	e-eq cells (e-eq Ac)$^{-1}$	Assumed	±25%
fs_{FER}^{PCS}	Cell yield of FER growing on PCS	0.180	e-eq cells (e-eq PCS)$^{-1}$	10	-
μ_{SRB}^{H2}	Max. growth of SRB growing on H_2	26.1	a^{-1}	Calculated	±25%
μ_{SRB}^{Ac}	Max. growth of SRB growing on Ac	40.3	a^{-1}	Calculated	±25%
μ_{MET}^{H2}	Max. growth of MET growing on H_2	23.2	a^{-1}	Calculated	±25%
μ_{MET}^{Ac}	Max. growth of MET growing on Ac	26.1	a^{-1}	Calculated	±25%
μ_{MOA}^{CH4H2O}	Max. growth of MOA growing on CH_4+H_2O	18.3	a^{-1}	Calculated	±25%
μ_{MOA}^{CH4CO2}	Max. growth of MOA growing on CH_4+CO_2	18.3	a^{-1}	Calculated	±25%
μ_{ACB}^{H2}	Max. growth of ACB growing on H_2	17.9	a^{-1}	Calculated	±25%
μ_{ACB}^{Ac}	Max. growth of ACB growing on Ac	18.3	a^{-1}	Calculated	±25%
μ_{FER}^{PCS}	Max. growth of FER growing on PCS	110.6	a^{-1}	Calculated	-

Table 4
(continued)

Parameter	Description	Baseline value	Units	Footnote ref.	Sensitivity
$\mu_{e_{SRB}}^{H2}$	Endogenous decay of SRB growing on H_2	0.04	a^{-1}	Calculated	±25%
$\mu_{e_{SRB}}^{Ac}$	Endogenous decay of SRB growing on Ac	0.22	a^{-1}	Calculated	±25%
$\mu_{e_{MET}}^{H2}$	Endogenous decay of MET growing on H_2	0.04	a^{-1}	Calculated	±25%
$\mu_{e_{MET}}^{Ac}$	Endogenous decay of MET growing on Ac	0.22	a^{-1}	Calculated	±25%
$\mu_{e_{MOA}}^{CH4H2O}$	Endogenous decay of MOA growing on CH_4+H_2O	0.11	a^{-1}	Calculated	±25%
$\mu_{e_{MOA}}^{CH4CO2}$	Endogenous decay of MOA growing on CH_4+CO_2	0.11	a^{-1}	Calculated	±25%
$\mu_{e_{ACB}}^{H_2}$	Endogenous decay of ACB growing on H_2	0.04	a^{-1}	Calculated	±25%
$\mu_{e_{ACB}}^{Ac}$	Endogenous decay of ACB growing on Ac	0.11	a^{-1}	Calculated	±25%
$\mu_{e_{FER}}^{GLU}$	Endogenous decay of FER growing on PCS	0.32	a^{-1}	Constrained	-
χ_{SRB}^{H2}	ASN Of SRB growing on H_2	1.0	Dimensionless	11	±75%
χ_{SRB}^{Ac}	ASN of SRB growing on Ac	1.0	Dimensionless	11	±75%
χ_{MET}^{H2}	ASN of MET growing on H_2	1.0	Dimensionless	11	±75%
χ_{MET}^{Ac}	ASN of MET growing on Ac	1.0	Dimensionless	11	±75%
χ_{MOA}^{CH4H2O}	ASN of MOA growing on CH_4 and H_2O	1.0	Dimensionless	11	±75%
χ_{MOA}^{CH4CO2}	ASN of MOA growing on CH_4 and HCO_3^-	1.0	Dimensionless	11	±75%
χ_{ACB}^{H2}	ASN of ACB growing on H_2	1.0	Dimensionless	11	±75%
χ_{ACB}^{Ac}	ASN of ACB growing on Ac	1.0	Dimensionless	11	±75%
χ_{FER}^{PCS}	ASN of FER growing on PCS	1.0	Dimensionless	11	-
$[m\Delta G_{ATP}]_{SRB}^{H2}$	Threshold of SRB growing on H_2	4.0	kJ mol^{-1}	Assumed	±25%
$[m\Delta G_{ATP}]_{SRB}^{Ac}$	Threshold of SRB growing on Ac	4.0	kJ mol^{-1}	Assumed	±25%
$[m\Delta G_{ATP}]_{MET}^{H2}$	Threshold of MET growing on H_2	4.0	kJ mol^{-1}	Assumed	±25%
$[m\Delta G_{ATP}]_{MET}^{Ac}$	Threshold of MET growing on Ac	4.0	kJ mol^{-1}	Assumed	±25%
$[m\Delta G_{ATP}]_{MOA}^{CH4H2O}$	Threshold of MOA growing on CH_4 and H_2O	4.0	kJ mol^{-1}	Assumed	±25%
$[m\Delta G_{ATP}]_{MOA}^{CH4CO2}$	Threshold of MOA growing on CH_4 and HCO_3^-	4.0	kJ mol^{-1}	Assumed	±25%

Table 4
(continued)

Parameter	Description	Baseline value	Units	Footnote ref.	Sensitivity
$[m\Delta G_{ATP}]_{ACB}^{H2}$	Threshold of ACB growing on H_2	4.0	kJ mol^{-1}	Assumed	±25%
$[m\Delta G_{ATP}]_{ACB}^{Ac}$	Threshold of ACB growing on Ac	4.0	kJ mol^{-1}	Assumed	±25%
$[m\Delta G_{ATP}]_{FER}^{PCS}$	Threshold of FER growing on PCS	4.0	kJ mol^{-1}	Assumed	-

1) Boudreau and Westrich (1984), Van Cappellen and Wang (1996); 2) Model fitted, highest value which allows hySR to proceed; 3) Visser and others (1993), van Bodegom and Scholten (2001), Schönheit and others (1982), Lovley and Klug (1986), Watson and others (2003); 4) Model fitted parameter; 5) Visser and others (1993), van Bodegom and Scholten (2001), Schönheit and others (1982), Lovley and Klug (1986), Fukuzaki and others (1990), Westermann and others (1989), Vavillin and others (1997), Oude Elferink and others (1994), Segers and Kengen (1998); Widdel (1988); 6) Lower value based on experiments by Nauhaus and others (2002); 7) Assumed to be lower than the H_2 half-saturation constant for MET; 8) No literature available as far as we are aware, assumed equal to Ac uptake by SRB; 9) Assumed value based on data in Pavlostathis and Giraldo-Gomez (1991). The model rates are insensitive to this parameter because PCS fermentation only controls the production of reactive intermediate; 10) Pavlostathis and Giraldo-Gomez (1991), Rittman and McCarty (2001); 11) $\chi = 1$ per electron transferred for anaerobic respiration, Jin and Bethke (2005).

$$\frac{fe}{2\,fs}\,SO_4^{2-} + \frac{5 + 3fs}{10\,fs}\,H^+ + HCO_3^- + 0.2NH_4^+ + \frac{2}{fs}\,H_2 \rightarrow 0.2C_5H_7O_2N + \frac{fe}{2\,fs}\,HS^- + \frac{10 + 3\,fs}{5\,fs}\,H_2O \quad (7)$$

Substituting the calculated values of *fs* and *fe* (table 4) gives:

$$9.7SO_4^{2-} + 10.5H^+ + HCO_3^- + 0.2NH_4^+ + 40.7H_2 \rightarrow 0.2C_5H_7O_2N + 9.7HS^- + 41.3H_2O \quad (8)$$

Thus, the synthesis of one C mole of SRB biomass via this pathway requires over 80 moles of electrons, which are supplied by H_2. Normally, by virtue of the imposed biomass stoichiometry, a source of nitrogen is required for organic matter synthesis. In the macrochemical equations of table 3, NH_4^+ is considered to be the nitrogen source. In the model, NH_4^+ is not considered as an independent variable, but is only used for calculating the standard Gibbs energy of biomass synthesis (see Appendix 3). Other elements, such as S and Fe, can be included into the biomass stoichiometry as required.

The rate of biomass growth must take into account all possible electron donors that can be used by the i*th* microbial group. The total growth rate, $r_{GR,i}$ (mol C L^{-1} a^{-1}), is thus given by:

$$r_{GR,i} = \sum_{E_D} r_{GR,i}^{E_D} \quad (9)$$

where $r_{GR,i}^{E_D}$ is the growth rate associated with the utilization of a specific electron donor E_D. Mathematically, $r_{GR,i}^{E_D}$ is obtained as:

$$r_{GR,i}^{E_D} = \mu_i^{E_D}.B_i.F_{T,i}^{E_D}.F_{K,i}^{E_D/A} \quad (10)$$

where $\mu_i^{E_D}$ (a^{-1}) is the maximum specific growth rate (Appendix 2), B_i the biomass (mol C L^{-1}), $F_{T,i}^{E_D}$ the thermodynamic driving force of the reaction (Appendix 4), and $F_{K,i}^{E_D/A}$ the kinetic driving force given by:

$$F_{K,i}^{E_D/A} = \frac{[E_D]}{K_{S,i}^{E_D} + [E_D]} \cdot \frac{[E_A]}{K_{S,i}^{E_A} + [E_A]} \quad (11)$$

where $K_{S,i}^{E_D}$ and $K_{S,i}^{E_A}$ are the half-saturation constants for E_D and E_A (mol L^{-1}), respectively. In the reaction network considered, the only E_A which is rate-limiting is SO_4^{2-}. Thus, for MET, MOA, ACB and FER equation (11) only includes the term dependent on the concentration of E_D.

The F_T and F_K terms are dimensionless and vary between 0 (no growth) and 1 (maximum growth). F_T depends on the Gibbs energy yield of the catabolic reaction, while F_K is a function of the uptake efficiencies of E_D and E_A by the microorganisms, as well as the local availabilities of E_D and E_A. The importance of including thermodynamic constraints is clearly illustrated for AOM (R_{11}, table 2), which is endergonic ($\Delta G^{o'} = +16.92$ kJ e-eq^{-1}) under standard conditions but exergonic under typical *in situ* conditions ($\Delta G_r = -1.18$ kJ e-eq^{-1}). Literature values for K_S (table 4) were selected taking into account the competitive hierarchy of SRB, MET and ACB observed in nature (Zinder, 1993). Note that accumulation of reaction products limits the reaction rate via the effect of the Gibbs energy of reaction (F_T, Appendix 4).

The rate of biomass decay is assumed to be specific to each biomass group and electron donor used for cellular synthesis and energy generation (Appendix 3). Hence, the total decay rate of a given biomass group i ($r_{DE,i}$, mol C L^{-1} a^{-1}) is:

$$r_{DE,i} = \sum_{E_D} r_{DE,i}^{E_D} \tag{12}$$

with

$$r_{DE,i}^{E_D} = \mu_{e,i}^{E_D}.B_i.\frac{r_{GR,i}^{E_D}}{r_{GR,i}} \tag{13}$$

where $\mu_{e,i}^{E_D}$ (a^{-1}) is the maximum decay rate when the organisms use E_D as electron donor, and the last term on the right-hand-side of the equation corresponds to the fraction of growth sustained by the given E_D. Finally, the net growth rate of biomass group i (mol C L^{-1} a^{-1}) is given by:

$$\frac{dB_i}{dt} = \sum_{E_D}\left[\mu_i^{E_D}.B_i.F_T.\frac{[E_D]}{K_{S,i}^{E_D}+[E_D]}.\frac{[E_A]}{K_{S,i}^{E_A}+[E_A]} - \mu_{e,i}^{E_D}.B_i.\frac{r_{GR,i}^{E_D}}{r_{GR,i}}\right] \tag{14}$$

The consumption and production of chemical species in the selected depth interval of the sediment can easily be derived from the growth rates and the reaction stoichiometries of the macrochemical equations in table 3. For example, from equation (8), the consumption of SO_4^{2-} by SRB growing on H_2 is equal to:

$$\frac{d[SO_4^{2-}]_{SRB}^{H2}}{dt} = -9.7\, r_{GR,SRB}^{H2} \tag{15}$$

Table 5 presents the biomass growth equations R_{7g}-R_{15g} corresponding to macrochemical reactions R_{7m}-R_{15m}. The differential equations constituting the mathematical model are solved using the stiff solver algorithm (ode15s) in Matlab® (release 6.5).

Global Sensitivity Analysis

As illustrated in table 4, the representation of the main microbial groups involved in methane dynamics in anoxic marine sediments introduces a large number of model parameters. Many of these parameters are fairly poorly known and, therefore, the simulation of the complex reaction dynamics incorporating a realistic reaction network for CH_4 cycling is only achieved at the cost of a significant increase of uncertainty in model predictions. Consequently, it is imperative to assess the sensitivity of the model output to the various parameters. To this end, a global sensitivity analysis is performed in order to identify the principal kinetic and thermodynamic parameters controlling AOM rates in coastal marine sediments.

For a complex reaction network model, testing the sensitivity parameter-by-parameter is time-consuming and overlooks potentially important synergistic or antagonistic interactions among parameters. Factorial design provides an alternative approach to perform a global sensitivity analysis on the complete set of model parameters. Detailed accounts of the theory of factorial design (Box, 1978; Montgomery, 1997), and numerous examples of applications in experimental and field studies can be found in the literature (Sahoo and others, 2000; Starzec and Andersson, 2002; Massumi and others, 2002; Dueri and Therrien, 2003; da Silva and others, 2004).

In factorial design, model sensitivity is determined by monitoring the response of a pre-defined model attribute (for example, a reaction rate or concentration) to perturbations of n model factors or parameters. In a two-level factorial analysis, each parameter is assigned a high and low value (or factor level). These values could, for

TABLE 5

Differential equations describing biomass growth on different electron donors. Five biomass groups are included (SRB, MET, MOA, ACB, FER). For clarity, the biomass and E_D identifiers have been removed from the F_T terms

Reaction	Growth equation
R_{7g}	$\frac{dB_{SRB}^{H2}}{dt} = \mu_{SRB}^{H2}.B_{SRB}.F_T.\frac{[H_2]}{K_{S-SRB}^{H2}+[H_2]}.\frac{[SO_4^{2-}]}{K_{S-SRB}^{SO4}+[SO_4^{2-}]} - \mu_{eSRB}^{H2}B_{SRB}.\frac{r_{GR-SRB}^{H2}}{r_{GR-SRB}}$
R_{8g}	$\frac{dB_{SRB}^{Ac}}{dt} = \mu_{SRB}^{Ac}.B_{SRB}.F_T.\frac{[Ac]}{K_{S-SRB}^{Ac}+[Ac]}.\frac{[SO_4^{2-}]}{K_{S-SRB}^{SO4}+[SO_4^{2-}]} - \mu_{eSRB}^{Ac}B_{SRB}.\frac{r_{GR-SRB}^{Ac}}{r_{GR-SRB}}$
R_{9g}	$\frac{dB_{MET}^{H2}}{dt} = \mu_{MET}^{H2}.B_{MET}.F_T.\frac{[H_2]}{K_{S-MET}^{H2}+[H_2]} - \mu_{eMET}^{H2}.B_{MET}.\frac{r_{GR-MET}^{H2}}{r_{GR-MET}}$
R_{10g}	$\frac{dB_{MET}^{Ac}}{dt} = \mu_{MET}^{Ac}.B_{MET}.F_T.\frac{[Ac]}{K_{S-MET}^{Ac}+[Ac]} - \mu_{eMET}^{Ac}.B_{MET}.\frac{r_{GR-MET}^{Ac}}{r_{GR-MET}}$
R_{11g}	$\frac{dB_{MOA}^{CH4H2O}}{dt} = \mu_{MOA}^{CH4H2O}.B_{MOA}.F_T.\frac{[CH_4]}{K_{S-MOA}^{CH4}+[CH_4]} - \mu_{eMOA}^{CH4H2O}.B_{MOA}.\frac{r_{GR-MOA}^{CH4H2O}}{r_{GR-MOA}}$
R_{12g}	$\frac{dB_{MOA}^{CH4CO2}}{dt} = \mu_{MOA}^{CH4CO2}.B_{MOA}.F_T.\frac{[CH_4]}{K_{S-MOA}^{CH4}+[CH_4]} - \mu_{eMOA}^{CH4CO2}.B_{MOA}.\frac{r_{GR-MOA}^{CH4CO2}}{r_{GR-MOA}}$
R_{13g}	$\frac{dB_{ACB}^{H2}}{dt} = \mu_{ACB}^{H2}.B_{ACB}.F_T.\frac{[H_2]}{K_{S-ACB}^{H2}+[H_2]} - \mu_{eACB}^{H2}.B_{ACB}.\frac{r_{GR-ACB}^{H2}}{r_{GR-ACB}}$
R_{14g}	$\frac{dB_{ACB}^{Ac}}{dt} = \mu_{ACB}^{Ac}.B_{ACB}.F_T.\frac{[Ac]}{K_{S-ACB}^{Ac}+[Ac]} - \mu_{eACB}^{Ac}.B_{ACB}.\frac{r_{GR-ACB}^{Ac}}{r_{GR-ACB}}$
R_{15g}	$\frac{dB_{FER}^{PCS}}{dt} = \mu_{FER}^{PCS}.B_{FER}.F_T.\frac{[PCS]}{K_{S-FER}^{PCS}+[PCS]} - \mu_{eFER}^{PCS}.B_{FER}$

instance, correspond to the upper and lower bounds of a specified confidence interval of the parameter. It is further assumed that the model response is approximately linear within the range of upper and lower factor levels. For n parameters, 2^n simulations are required to resolve the model sensitivity (termed the "effect") to all possible parameter combinations. The mathematical procedure is based on applying Yates' algorithm to the 2^n responses generated by the model (Box, 1978; Montgomery, 1997).

To illustrate the procedure, table 6 shows a two-level factorial analysis for three parameters (A, B, C). A total of (2^3 =) 8 model runs are required to encompass all combinations of the three parameters, each at two levels. The notations "+" and "–" in the design matrix indicate whether the parameters are assigned their high or low level values, respectively. Run 2, for example, evaluates the effect of parameter A only (*a*), while Run 8 assesses the combined effect of all three parameters (*abc*). Of the seven degrees of freedom ($2^n - 1$) of the factorial analysis, three are associated with the first-order effects of the individual parameters A, B and C. The other four are associated with second-order (AB, AC, BC) and third-order (ABC) interactions. By convention, the combination of all parameters at their lowest level is termed (1).

Each of the eight simulations results in a particular value of a user-specified model output (that is, the response). The response values in table 6 are assigned arbitrarily for

TABLE 6

Design of a 2^3 two-level factorial analysis, showing the estimates of the main effects for the parameter combinations

Run	A	B	C	Treatment combination	Response	(1)	(2)	(3)	Effect	Estimate of Effect $(3)/2^{n-1}$
1	–	–	–	(1)	10	13	21	22	-	-
2	+	–	–	*a*	3	8	1	-52	*A*	-13.0
3	–	+	–	*b*	15	8	-29	-20	*B*	-5.0
4	+	+	–	*ab*	-7	-7	-23	-26	*AB*	-6.5
5	–	–	+	*c*	7	-7	-5	-20	*C*	-5.0
6	+	–	+	*ac*	1	-22	-15	6	*AC*	1.5
7	–	+	+	*bc*	5	-6	-15	-10	*BC*	-2.5
8	+	+	+	*abc*	-12	-17	-11	4	*ABC*	1.0

the purpose of illustration. (In the present study, the logical model response is the net rate of AOM.) The response for each run is a function of the effect of individual or combinations of parameters. Since each parameter appears in more than one run (for example parameter A appears in combinations *a*, *ab*, *ac* and *abc*) the responses are non-unique to an individual parameter. Therefore, the contribution of each individual parameter or combination thereof on the response is determined as the "effect", which is the relative importance of the parameter(s) on the response. The Yates algorithm is used to derive the effects of the parameter combinations from the model responses (Box, 1978; Montgomery, 1997). In table 6, the upper half of column (1) is obtained by adding the responses of successive pairs of combinations, thus, $10 + 3 = 13$, $15 + (-7) = 8$, $7 + 1 = 8$ and $5 + (-12) = -7$. The lower half of column (1) is obtained by changing the sign of the first entry in each response pair, so that $-10 + 3 = -7$, $-15 + (-7) = -22$, and so on. Column (2) is derived from column (1) in the same way as column (1) is obtained from the response column. Column (3) is similarly obtained from column (2), and so on until column (n) in a 2^n factorial design. Finally, the estimates of the effects are calculated by dividing the entries in the last column (n) by 2^{n-1}.

Next, a normal probability plot is used to rank the parameter sensitivities derived with the Yates algorithm. The estimates of the effects $y_{(i)}$ (final column, table 6) are arranged in ascending order from $y_{(1)}$ through to $y_{(m)}$ (where $m = 2^n - 1$), and plotted against the cumulative frequency, $P_i = 100(i-0.5)/m$ for $i = 1, 2, \ldots m$. If the change from lower to upper levels of the parameters does not have a major effect on the model output, then the response of the model should exhibit a normal variation about a fixed mean of zero. The effects should then define a straight line on a normal probability plot. If most effects indeed fall on a straight line, the assumption of a normal distribution is reasonable. Effects that deviate significantly from the linear trend, however, correspond to parameters or combinations of parameters, which have a significant impact on the model response. These are therefore the most critical model parameters to be constrained. For the example in table 6, such an analysis reveals that the model outcome is most sensitive to parameter A and parameter combination AB.

In our model there are 48 adjustable parameters. A global sensitivity analysis including all 48 parameters would require $2^{48} = 3 \times 10^{14}$ model runs, with a prohibitive simulation time approaching 6×10^9 years on the first author's personal computer. To reduce computational time significantly, the parameters are divided in 6 groups of 8

parameters, according to parameter type ($m\Delta G_{ATP}$, χ, *fs*, K_S, μ, μ_e, table 4). As the emphasis of the sensitivity analysis is on the internal dynamics of the reaction network, the external forcing parameters of the reaction system, that is, the influx of PCS, followed by the production of fermentation products (H_2 and Ac), are excluded from the analysis. The sensitivity ranges of the parameters tested are ± 25 or ± 75 percent (table 4), with all parameters within a given group varied over the same range. By changing each parameter by the same proportion, the relative importance of the individual processes in determining the model response can be assessed. The purpose here is thus to test the relative sensitivity of the model response to all parameters, rather than to investigate the variability in response arising from experimental uncertainty or natural variability of parameters.

A full two-level factorial analysis of each of the 6 parameter groups requires (2^8 =) 256 runs, which is still computationally demanding. Therefore, we only consider first-order (individual parameters) and second-order (combinations of two parameters) effects, using a fractional factorial design. The choice of this design represents a trade-off between computational time and desired order of parameter combinations to investigate. The design used here is a 2^{8-3} factorial, which is ⅛ fraction of 8 factors in 32 runs. With this design, some second-order parameter effects are non-unique, for example the *AB* effect could be indistinguishable from *AC*. The main effects, however, are unique. The structure of the design matrix (table 6) for fractional factorials is straightforward (Box and others, 1978; Montgomery, 1997). In addition, Yates algorithm for a 2^{8-3} design is applied as before, but considering the data as having been obtained from a complete factorial in (8 − 3=) 5 factors, implying 32 runs. Using the fractional design, each group sensitivity analysis requires approximately 4 hrs on a 2.8 GHz personal computer.

MODEL APPLICATION

Baseline Simulation

This section describes the baseline simulation using the parameters listed in table 4. The simulation is run forward in time, until the yearly-averaged total biomass reaches a steady state value. From that point on, the chemical concentrations, biomass and process rates exhibit stable, repeating yearly cycles (figs. 3A-F). To facilitate the discussion of the observed temporal changes, the yearly cycles are divided into winter and summer periods of equal lengths (fig. 1). Fluctuations in process rates are interpreted in terms of variations in the thermodynamic (F_T, fig. 3G, Appendix 4) and kinetic (F_K, fig. 3H, eq 10) driving forces. Note that F_T and F_K are dimensionless parameters varying between 0 and 1. The total driving force for growth, F_{TOT} (fig. 3I), is defined as the product of F_T and F_K. When F_{TOT} approaches unity, corresponding microorganisms grow at a rate close to their maximum specific rate (μ).

Biomasses.—Fermentative bacteria (FER) exhibit the highest biomass ($\sim 1.1\times10^{-4}$ mol C L^{-1}), followed by SRB, MOA, MET and ACB (table 7). Assuming a value of 19 fgC $cell^{-1}$ (Schippers and others, 2005), mean total biomass (fig. 3A, table 7) amounts to 2.2×10^{-4} mol C L^{-1}, or 1.4×10^{8} cells cm^{-3}. This value falls within the range of 0.45-2.20 × 10^8 cells cm^{-3} given by Whitman and others (1998) for subsurface sediments (0.1 – 10 m), but is roughly one order of magnitude lower than cell counts ($\sim 5.0\times10^{9}$ cells cm^{-3}) reported by Luna and others (2002) for coastal marine sediments. However, the modeled biomasses correspond only to the metabolically active (alive, non-dormant) microorganisms, which may constitute only a small fraction of the total biomass (Luna and others, 2002). MOA biomass (table 7) compares also very favorably to cell counts reported for the SMTZ in Eckernförde Bay (3.8-5.1×10^{7} cells cm^{-3}; Treude and others, 2005). The mean annual rate of carbon assimilation into biomass equals 9.60×10^{-5} mol C L^{-1} a^{-1}, which leads to a microbial

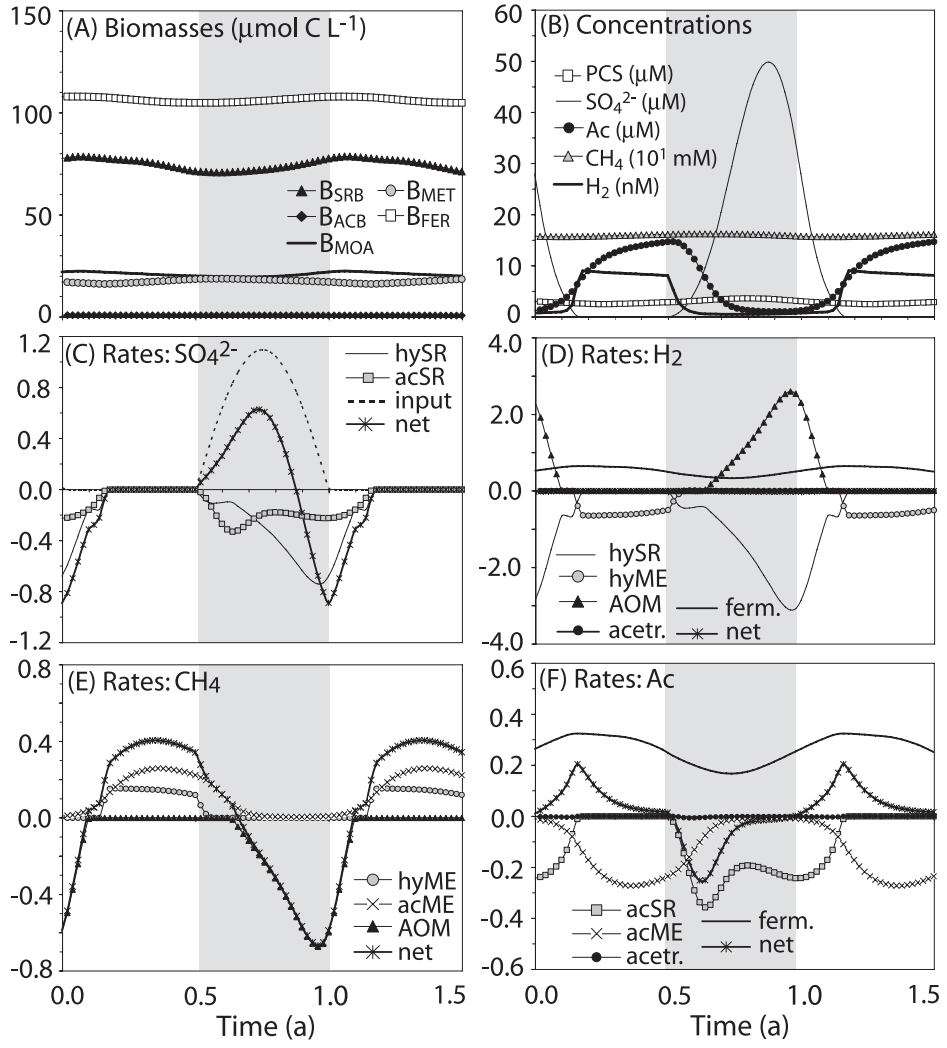

Fig. 3. Baseline simulation using the parameter values in table 4. The results displayed correspond to a 1.5 year duration after steady state with respect to yearly averaged biomass is attained. (A) Biomasses (μmol C L^{-1}), (B) chemical concentrations (see legend for units), (C-F) process rates and net rates (nmol cm^{-3} d^{-1}),

turnover time of (2.2×10^{-4} / 9.60×10^{-5}=) 2.3 a. This value is comparable to those reported elsewhere for a range of marine sediments (Whitman and others, 1998; Schippers and others, 2005).

The model predicts small intra-annual variability of the biomasses (fig. 3A), despite large changes in process rates. SRB biomass fluctuates by ±20 percent over a half-year period, which, assuming exponential growth, leads to an apparent first-order growth rate of (ln(1.20)/0.5=) 0.36 a^{-1}, or an *in situ* doubling time of (ln(2)/0.36=) 1.9 a. Similarly, the *in situ* doubling time for the MOA is 2.6 a. This value is substantially longer than the 3+ months reported by Girguis and others (2005). Yet, their experimental conditions differ significantly from those representative of our baseline simulation. In our case, the sluggish growth of the modeled MOA biomass results from the intense competition for energy substrates and from the restricted six-month

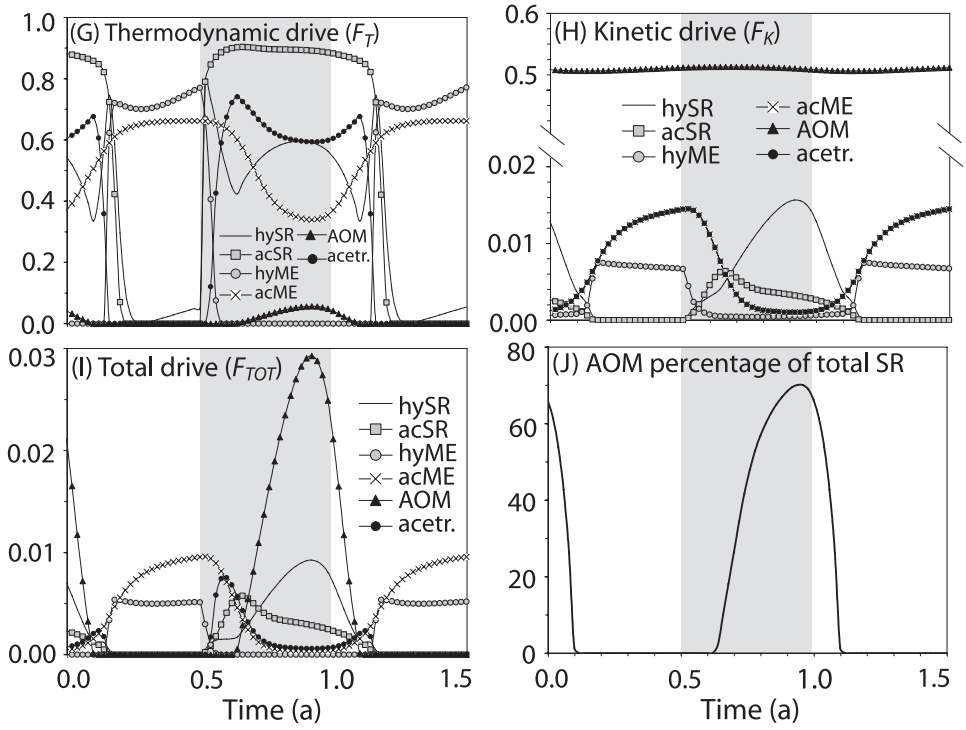

Fig. 3 (continued). (G) thermodynamic driving forces for catabolic pathways, F_T (eq A-19), (H) kinetic driving forces, F_K (eq 11), (I) total pathway limitations, F_{TOT} ($=F_T \times F_K$), and (J) fraction of SR coupled to AOM (%). Positive process rates indicate production and negative rates indicate consumption. Key: hySR = hydrogenotrophic sulfate reduction (R_{7m}, table 3), acSR = acetotrophic sulfate reduction (R_{8m}), hyME = hydrogenotrophic methanogenesis (R_{9m}), acME = acetotrophic methanogenesis (R_{10m}), AOM = anaerobic methane oxidation (R_{11m}), acetr. = acetotrophy (R_{14m}), ferm. = fermentation (R_{15m}). The winter period is indicated by the shading.

growth period. In contrast, in the core incubation experiments of Girguis and others (2005) MOA biomass growth occurred under high flow rates of SO_4^{2-} and CH_4.

The small changes in modeled biomasses compared to substrate turnover illustrates that variation in the cell-specific activities is mainly controlling the reaction dynamics (Thullner and others, 2005). The assumption of steady state biomass is, therefore, a valid approximation for modeling the anaerobic AOM reaction network over seasonal time scales. It is probable that this conclusion can be generalized to anaerobic sediments where there is significant kinetic and thermodynamic limitation of substrate catabolism. In these systems, diagenetic reactive-transport models can justifiably employ maximum substrate turnover rates to simulate microbial processes (Van Cappellen and Wang, 1996).

PCS.—PCS concentrations are relatively constant throughout the year (~3.0 μM; fig. 3B). As a comparison, Burdige and others (2000) reported dissolved carbohydrate (DCHO) concentrations of 20 to 130 μM in subsurface sediments of Chesapeake Bay. In these sediments, individual monomeric neutral sugars represented 30 to 50 percent of the total DCHO concentration. More extreme DCHO concentrations of >1000 μM were measured by Arnosti and Holmer (1999) in the organic-rich Cape Lookout Bight. The environmental controls on DCHO concentrations and cycling in marine sediments are poorly understood (Burdige and Gardner, 1998), particularly with regard to

TABLE 7

Mean biomass concentrations, rates and cell-specific rates simulated for the 5 microbial groups. The rates refer to the production/consumption of the chemical compound listed in parenthesis

Species	(i) Biomass (mol C L^{-1})	(ii) Biomass[1] (cells cm^{-3})	(iii) Rate (mol cm^{-3} d^{-1})	(iv) Cell-specific rate[2] (fmol $cell^{-1}$ d^{-1})
SRB (SO_4^{2-})	7.46×10^{-5}	4.71×10^{7}	5.28×10^{-10}	0.011
MOA (CH_4)	2.08×10^{-5}	1.32×10^{7}	3.41×10^{-10}	0.026
MET (CH_4)	1.76×10^{-5}	1.11×10^{7}	2.35×10^{-10}	0.021
ACB (Ac)[3]	8.29×10^{-7}	5.23×10^{5}	1.93×10^{-12}	0.004
FER (C)	1.06×10^{-4}	6.71×10^{7}	1.54×10^{-10}	0.002
total	2.20×10^{-4}	1.39×10^{8}	-	-

[1]Calculated from column (i) assuming a cellular carbon content of 19 fg C $cell^{-1}$ (Schippers and others, 2005).
[2]Calculated by dividing column (iii) by column (ii).
[3]Refers to Ac consumption via acetotrophy only (R_{14m}, table 3).

seasonality (Alperin and others, 1994). Nonetheless, in this study we can conclude that the low simulated PCS concentrations reflect fermentative control on DCHO, as suggested by Burdige and others (2000) with regard at nearshore marine sediments. The thermodynamic drive (F_T) for fermentation is always >0.99 (data not shown).

Model-derived seasonal PCS turnover times vary from 13 d in summer to almost 33 d in winter. These compare favorably with those of Alperin and others (1994), who derived seasonal turnover times for nonacid-volatile dissolved organic carbon (NAVDOC) varying from 7 d (summer) to 40 d (winter) at the approximate mean depth of the SMTZ (15 cm, Hoehler and others, 1994) in Cape Lookout Bight. Thus using glucose as a proxy yields a reactivity of PCS that is realistic.

Sulfate.—The SO_4^{2-} concentration (fig. 3B) shows a clear annual cycle, with a maximum of 49.8 μM in winter in response to the imposed enhanced supply of SO_4^{2-} into the window of observation (Klump and Martens, 1989; fig. 1). During winter, the influx of SO_4^{2-} sustains hydrogenotrophic sulfate reduction (hySR; R_{7m}, table 3) and acetotrophic sulfate reduction (acSR; R_{8m}, table 3) (fig. 3C). The rate of hySR (R_{7m}) exhibits a central peak at the winter-summer transition (time = 1.0 a) bound by two shoulder peaks (fig. 3C), also observed in the rate of H_2 consumption by SO_4^{2-} (fig. 3D). hySR is the major sink for SO_4^{2-} in winter (61.2%), with acSR (R_{8m}) consuming the remaining 38.8 percent.

The combined cell-specific rate of hySR and acSR equals 0.011 fmol SO_4^{2-} $cell^{-1}$ d^{-1} (table 7), or approximately 0.6 mmol SO_4^{2-} g (dry cell mass)$^{-1}$) d^{-1} (assuming $1/19\times10^{-15} = 5.3\times10^{13}$ cells (g dry cell mass)$^{-1}$). This value is similar to the 0.03 fmol $cell^{-1}$ d^{-1} reported for Arctic sediment at ~10 cm depth by Ravenschlag and others, 2000. Nauhaus and others (2005) determined higher cell-specific rates of 1 and 20 mmol SO_4^{2-} g (dry cell mass)$^{-1}$) d^{-1} for microbial mats (Black Sea) and methane-oxidizing consortia (Hydrate Ridge), respectively. The transport regimes in these systems are, however, not the same as those of typical nearshore sediments and rates are thus difficult to compare.

Two-thirds of hySR is coupled to hydrogen production by AOM (see below), implying that oxidation of fermentation products also represents a significant proportion of total SR (Iversen and Blackburn, 1981; Iversen and Jørgensen, 1985). An

imbalance between SO_4^{2-} production and consumption rates creates a time-lag of ~1 month between the maximum SO_4^{2-} input (fig. 3C) and SO_4^{2-} concentration (fig. 3B). This imbalance is due to kinetic (fig. 3H), rather than thermodynamic (fig. 3G), limitation of hySR, as F_K only reaches maximum values of around 0.02, compared to much higher values of F_T (0.4 – 0.8), throughout winter. As a result, non-zero SO_4^{2-} concentrations persist during early summer (fig. 3B).

Hydrogen.—The dynamic variations in H_2 production and consumption (fig. 3D) are not reflected in H_2 concentrations due to rapid H_2 turnover (Cord-Ruwisch and others, 1988; Lovley and Goodwin, 1988). Nonetheless, a significant difference is observed between summer (7.5 nM) and winter concentrations (0.44 nM). The contrasting summer and winter H_2 concentrations reflect hyME and hySR as terminal electron accepting processes, respectively (Lovley and Goodwin, 1988). The lower winter H_2 concentrations result from the higher affinity of SRB for H_2 than for MET (Hoehler and others, 1998; Jakobsen and others, 1998; Watson and others, 2003). Therefore, during winter, methanogenesis stops because MET are outcompeted by the SRB for Ac and H_2 (Sansone and Martens, 1982). The subsequent increase in hySR (R_{7m}) causes an increase in the thermodynamic drive for acetotrophy (R_{14m}; fig. 3G; $F_T = \sim 0.7$). Acetotrophy and, more importantly, fermentation supply the H_2 which result in the side peaks in hySR noted earlier (figs. 3C and 3D). Whereas fermentation (R_{15m}) provides a continuous source of H_2 throughout the year (~0.5 nmol H_2 cm^{-3} d^{-1}), production of H_2 via acetotrophy is comparably trivial and decreases throughout winter because of competition for Ac by acSR (fig. 3C).

However, by far the most important pathway of H_2 production is AOM (R_{11m}). At its peak, AOM produces 2.6 nmol H_2 cm^{-3} d^{-1} (fig. 3D), and sustains the high rates of hySR (R_{7m}) in winter. The H_2 transfer from AOM to hySR is akin to the interspecies H_2 transfer believed to occur within SRB-MOA aggregates (Hoehler and others, 1994; Boetius and others, 2000; Sørensen and others, 2001). Toward the start of summer, when SO_4^{2-} is depleted, AOM is no longer thermodynamically viable ($F_T = 0$, fig. 3G) and H_2 concentrations rapidly increase to 7.5 nM, at which point hydrogenotrophic methanogenesis (hyME; R_{9m}) becomes thermodynamically spontaneous ($F_T > 0$; fig. 3G).

Methane.—Production and consumption of CH_4 shows the expected summer and winter alternation, although a time lag is observed: production extends into early winter and consumption into early summer (fig. 3E). The contribution of AOM to CH_4 cycling leads to a maximum consumption rate of 0.67 nmol CH_4 cm^{-3} d^{-1} (fig. 3E), which is comparable to values reported for the base of the SMTZ in Cape Lookout Bight (Martens and others, 1998), Eckernförde Bay (Martens and others, 1999; Treude and others, 2005) and Kysing Fjord (Iversen and Blackburn, 1981).

The cell-specific rate of AOM equals 0.026 fmol CH_4 $cell^{-1}$ d^{-1} (table 7). For comparison, the seasonal range (March-September) of mean volumetric AOM rates reported by Treude and others (2005) for 3 sediment cores from Eckernförde Bay (~0.8 – 55.6 nmol cm^{-3} d^{-1}) is equivalent to cell-specific rates of roughly 0.02 to 0.12 fmol CH_4 $cell^{-1}$ d^{-1}. In addition, if one assumes that biomass remains constant in Eckernförde Bay sediments, then the wide range in seasonal AOM rates reinforces the importance of cell-specific activity rather than cell numbers in determining substrate turnover in anaerobic sediments.

Throughout the year, F_K for AOM is high (0.51, fig. 3H) due to sustained availability of CH_4. However, the sufficiently low H_2 concentrations needed for thermodynamically spontaneous AOM (R_{11m}) only occur during winter (fig. 3G). Even during winter, however, AOM only proceeds at around 3.0 percent of its potential maximum rate (fig. 3I), mainly due to thermodynamic limitation (fig. 3G). The model predicts that AOM using HCO_3^- as electron acceptor (R_{12m}) is never thermodynami-

cally favorable (data not shown), as predicted by Hoehler and others (1994). For typical CH_4 (1.5 mM) and HCO_3^- (10 mM) concentrations, the Ac concentration would need to decrease by almost 2 orders of magnitude from the baseline winter levels (~1.0 μM) for this pathway to be thermodynamically spontaneous.

The fraction of SR invested in AOM via hySR reaches a peak in late winter, with values up to 70 percent (fig. 3J), and then decreases rapidly to zero in early summer. Comparison of figures 3D, 3E and 3J shows that the temporal evolution of the proportion of SR coupled to AOM directly follows the production of H_2 by AOM. This result reflects the relatively large influx of SO_4^{2-} to the window-of-observation, during the period AOM is thermodynamically feasible. Hence, coupling of AOM and SR is not limited by SO_4^{2-} availability during that time. While the result of figure 3J is dependent on the particular forcings imposed in the baseline simulation, it nevertheless illustrates that large spatio-temporal variations in the fraction of SO_4^{2-} channeled into AOM can be expected in coastal marine sediments.

Variations in the rate of CH_4 production by hyME are strongly controlled by the seasonal oscillation of the thermodynamic driving force, F_T (fig. 3G), in response to the variations in the local H_2 concentration (fig. 3B). In contrast, the variations of F_T for acME are consistently high (between 0.34 and 0.66). Both pathways, however, are always severely limited by substrate availability (fig. 3H) and, therefore, proceed at <1 percent of their potential maximum rates (fig. 3I). Together with the relatively low influx of PCS imposed in the baseline simulation, the strong limitation of hyME and acME results in relatively low rates of CH_4 production (fig. 3E). Such low rates are typical for the SMTZ, where methane production tends to be inhibited by the presence of SO_4^{2-} (Crill and Martens, 1986; Whiticar and others, 1986; Blair and Carter, 1992; Martens and others, 1998; Avery and Martens, 1999). Methane dynamics in the window-of-observation are thus characterized by fairly sluggish methanogenesis and AOM rates (Jørgensen and others, 2001), which explains the fairly stable CH_4 concentrations observed throughout the year (fig. 3B).

Acetate.—Acetate is a key reactive intermediate for SR and methanogenesis in marine sediments (Winfrey and Ward, 1983). Its concentration often reflects the dominant terminal electron accepting process, in a similar way to H_2 (Crill and Martens, 1986; Hoehler and others, 1999). Modeled Ac concentrations are elevated in summer (14.7 μM, fig. 3B), when SO_4^{2-} is absent, and low throughout winter (1.0 μM), when SO_4^{2-} is present. Alperin and others (1992) reported Ac concentration in SO_4^{2-}containing sediments between 1 to 9 μM. Because of the relatively low daily flux of PCS imposed in the simulations (0.14 nmol cm^{-3} d^{-1}; fig. 1), the millimolar Ac concentrations observed below the SO_4^{2-} penetration depth in nearshore sediments are not simulated (Sansone and Martens, 1982; Crill and Martens, 1986; Alperin and others, 1992).

There is a notable peak of net Ac production in early summer (0.21 nmol Ac cm^{-3} d^{-1}, fig. 3F), when SO_4^{2-} becomes depleted and H_2 concentrations increase. However, the model does not reproduce the often-observed transitional 1 to 2 month peak of elevated Ac concentrations, which accompanies the winter-spring transition (Sansone and Martens, 1982; Alperin and others, 1992). Isotopic and incubation experimental evidence suggests that this period of Ac accumulation may be mostly due to a temporary decoupling of Ac production by ACB (R_{13m}) and Ac consumption via acME (Alperin and others, 1992; Alperin and others, 1994; Hoehler and others, 1999; Fey and others, 2004). Instead, in the model H_2-utilizing ACB are unable to compete with the MET at any time, despite similar growth rates and saturation constants (table 4). This is because ACB using H_2 gain even less energy than MET (table 2), and are always thermodynamically inhibited (F_T = 0, data not shown). However, Ferdelman and others (1997) noted high numbers of H_2-utilizing acetogenic bacteria in Chilean

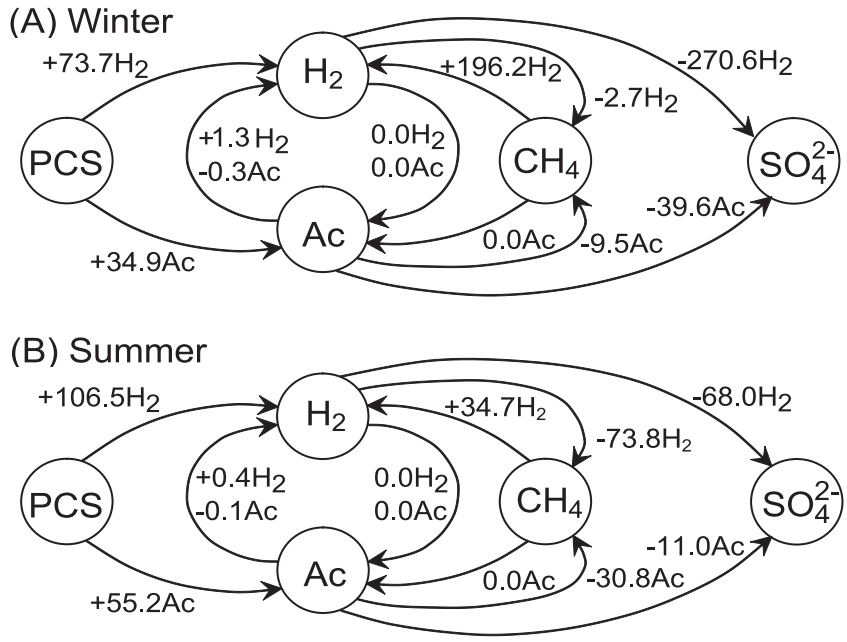

Fig. 4. Mass balances of H_2 and Ac in the baseline simulation averaged over the 6 months of (A) winter and (B) summer. Primary carbon substrate (PCS) and sulfate (SO_4^{2-}) are supplied externally to the sediment in the window-of-observation. Average annual rates are given in nmol cm^{-3} a^{-1}. Zero values are assigned to rates less than ± 0.001 nmol cm^{-3} a^{-1}. Note that H_2 consumption by methanogenesis and H_2 production by AOM never occur simultaneously. Their simultaneous occurrence in the figure is thus the result of temporal averaging and of the definition of the summer-winter transition which is based on temperature rather than on AOM viability.

sediments, whilst methanogenic organisms appeared to be less prominent. The representation of the ACB in our model may be too simplified, and fail to account for the wide scope for substrate utilization of ACB, including sugars, methylamines and other methylated compounds (Drake, 1994). Ferdelman and others (1997) even concluded that ACB may provide an intermediate metabolic pathway between fermentation and SR, at the expense of methanogenesis.

As a consequence of thermodynamic inhibition of acetogenesis, there is high thermodynamic drive for acetotrophy throughout the year, with cellular rates for the ACB of 0.004 fmol Ac $cell^{-1}$ d^{-1} (table 7). However, F_{TOT} shows that acetotrophy is limited to 0.8 percent of its maximum rate at the start of winter (t = 0.6 a, fig. 3I) because of low F_K (fig. 3H), which reflects the extent to which MET and SRB are able to compete effectively against the ACB for Ac. Acetotrophy is forced by the low H_2 concentrations due to hySR in winter and by hyME in summer. In support of these model predictions, laboratory experiments have shown that acetogenic ACB can operate in reverse in syntrophic partnership with a methanogen (Lee and Zinder, 1988). Recent isotopic labeling studies further suggest that this mechanism probably accounts for approximately half of acetate oxidation in the freshwater sediments of Lake Kinneret (Israel) (Nüsslein and others, 2001).

Mass balances.—The contrasting winter and summer chemical dynamics in the sediment interval considered are summarized in figure 4. As an example, let us consider H_2 in winter (fig. 4A). Of the total H_2 production during the 6 winter months

(271.2 nmol cm^{-3}), SRB consume (270.1/271.2=) 99.8 percent, while hyME (R_{9m}) is responsible for the remaining 0.2 percent. No H_2 is used for acetogenesis. Therefore, SR constitutes the major sink for H_2 in the sediment during winter. Production of H_2 via AOM (196.2 nmol cm^{-3}) represents (196.2/271.2×100=) 72.4 percent of total H_2 production and, therefore, (196.2/270.1×99.8=) 72.4 percent of total winter hySR. As total SR during winter is 97.0 nmol SO_4^{2-} cm^{-3} and hySR (R_{7m}) is 59.4 nmol SO_4^{2-} cm^{-3}, (59.4/97.0×100=) 61.2 percent of total SR is attributable to hySR, with acSR (R_{8m}) accounting for the remainder (data not shown). Thus, (72.4%×0.612=) 44.3 percent of the total SR is coupled to AOM. Acetotrophy (R_{14m}) and H_2 production from fermentation (R_{15m}) provide 0.5 percent and 27.2 percent of H_2 in the sediment window-of-observation, respectively, and constitute 0.3 percent and 16.6 percent of total SR.

The same calculations for summer illustrate the large changes in the terminal electron accepting pathways of the sediment (fig. 4B). Because SO_4^{2-} concentrations extend in the first month of summer (fig. 3B), AOM is still significant, but now only accounts for 24.5 percent of hySR (R_{7m}) and 16.4 percent of total SR. The sediments are notably more methanogenic than in winter, with hyMe (R_{9m}) accounting for 52.0 percent of total H_2 consumption. The remaining 48.0 percent can be attributed to hySR. Again, acetogenesis (R_{13m}) does not influence the H_2 budget in this sediment depth interval. The fraction of total Ac consumption by acetotrophy decreases from 0.7 percent (winter) to 0.3 percent (summer), and the fraction of total Ac consumption by SRB decreases from 80.0 percent to 26.2 percent. The surplus sediment Ac stock in summer is channeled to methanogenesis, which consumes 73.5 percent of total Ac production, compared to only 19.3 percent in winter.

Global Sensitivity Analysis

The results of the fractional factorial analysis are displayed as probability plots for each parameter type ($m\Delta G_{ATP}$, χ, *fs*, K_S, μ, μ_e) included in the model (fig. 5). The data points represent either a main effect of a single parameter or a combined effect from second-order interactions between 2 parameters. The model response used in the sensitivity analysis is the mean annual rate of AOM after steady state of the mean annual biomass has been reached. The straight lines on the individual plots correspond to the normal statistical distribution. Points lying away from the lines represent parameter(s) causing a significant response in the rate of AOM, and are thus the most sensitive at the levels tested. These parameters are labeled on the plots. According to the sensitivity analysis, however, second-order effects are not important, with one exception (see below).

Kinetic and growth parameters.—Among the half-saturation constants, K_{S-SRB}^{H2} and K_{S-MET}^{Ac} have the largest effects on AOM rates, while K_{S-SRB}^{SO4} and K_{S-MET}^{H2} are also notably sensitive. The 4 corresponding points lie to the left of the normal distribution curve, meaning that an increase in these parameter values results in a decrease in AOM rates. Conversely, K_{S-ACB}^{Ac} lies to the right of the line, indicating that increasing this parameter increases the rate of AOM. A striking result is that K_{S-MOA}^{CH4H2O} and K_{S-MOA}^{CH4CO2} do not exert a significant control on AOM, at the tested range of sensitivity, corroborating the large kinetic drive for AOM observed in figure 3H.

Results for the growth rate parameters μ and μ_e indicate that increased rates of hySR (R_{7m}), hyME (R_{9m}), acME (R_{10m}) and AOM (R_{11m}) promote methane oxidation, whereas higher rates of acetotrophy (R_{14m}) have the opposite effect. It is important to note that most of the parameter values μ and μ_e used in the model simulation are predicted from thermodynamic principles (see Appendices). In particular, the values listed in table 4 constitute the first estimates of the growth kinetics of MOA. Experimental determination of μ and μ_e under *in situ* conditions is challenging, and one often has to resort to growth proxies such as ATP concentration or enzymatic activity (Novitsky,

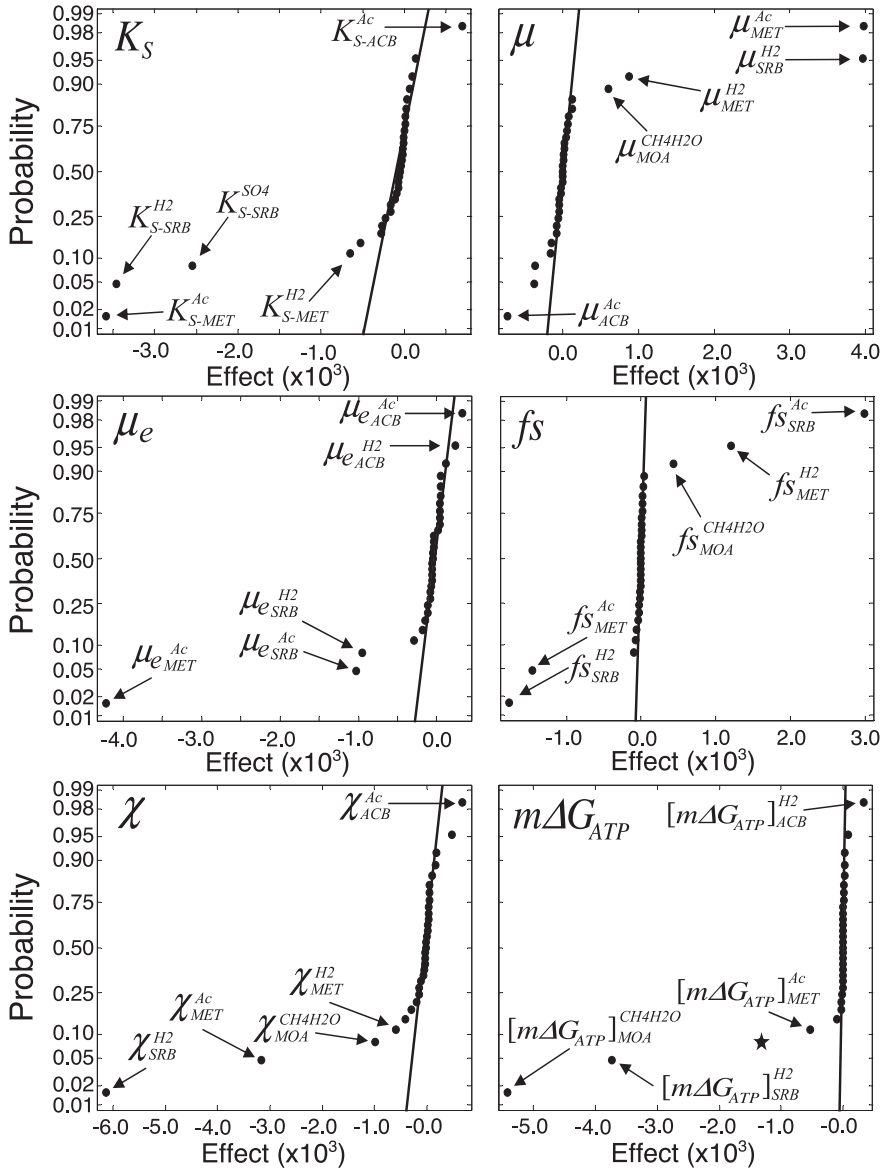

Fig. 5. Normal probability plots of the factorial sensitivity analyses grouped according to parameter type. The star on the bioenergetic threshold plot ($m\Delta G_{ATP}$) denotes the combined interaction of $[m\Delta G_{ATP}]^{H2}_{SRB}$ and $[m\Delta G_{ATP}]^{CH4H2O}_{MOA}$. See text for complete discussion.

1987; Poremba and Hoppe, 1995; Wellsbury and others, 1996; Luna and others, 2002; Haglund and others, 2003). Additionally, intermittent nutrient limitation (Luna and others, 2002) and dormancy (Kaprelyants and others, 1993) alters the physiological condition of the microbes and thus creates short-term divergence in growth and decay rates (Harder, 1997). However, it is worth stressing that AOM rates are relatively insensitive to the values of μ and μ_e for MOA. On the basis of the near-steady state biomasses observed in the simulations (fig. 3A), the uncertainties in μ and μ_e for SRB

and MET can be merged into bulk maximum substrate turnover rates (v_{max}, Lovley and Goodwin, 1988). For anoxic marine sediments, the steady state biomass approximation allows one to significantly reduce the number of model parameters required, without significantly affecting the model-predicted reaction dynamics.

On first examination, the sensitivity results for the cellular yield parameters, *fs*, display a variety of effects that sometimes contrast with the findings for K_S, μ and μ_{e^-}. For example, the effects of fs^{Ac}_{MET} and fs^{H2}_{SRB} appear to contradict those of $\mu_{e^-_{SRB}}$ and $\mu_{e^-_{MET}}$, as the former effects lie to the left of the normal distribution curve, whereas the decay rate results suggest that higher acME and hySR biomasses would promote AOM. On the other hand, the effects of fs^{H2}_{MET}, fs^{Ac}_{SRB} and fs^{CH4H2O}_{MOA} appear to agree with the corresponding sensitivity results for K_S, μ and μ_{e^-}. This reasoning presumes that cellular yield is a direct proxy for biomass, however. As shown below, careful analysis and further simulations (not shown), help resolve the apparent contradictions in terms of H_2 and Ac concentrations.

Firstly, for fs^{Ac}_{MET}, recall that a higher cell yield leads to lower catabolic uptake of Ac per mol C biomass synthesized via the stoichiometric coefficient for Ac of ½ *fs* (R_{10m}, table 3). Increasing fs^{Ac}_{MET} thus increases Ac availability in the pore water, leading to higher rates of acSR and, by implication, lower rates of hySR. As discussed previously, AOM is dependent on sustained hySR to lower the H_2 concentration to the level required to make AOM thermodynamically spontaneous ($F_T > 0$). For this reason, fs^{Ac}_{MET} lies to the left of the normal distribution curve for the tested range. A similar interpretation is applicable to fs^{H2}_{SRB}.

For fs^{H2}_{MET}, however, the same argument does not apply: fs^{H2}_{MET} lies to the right of the curve, but increasing fs^{H2}_{MET} should increase the pore water H_2 concentration (R_{9m}, table 3), thus leading to lower AOM rates. Further investigation in fact shows that higher pore water H_2 concentrations in summer from increasing fs^{H2}_{MET} favor AOM by inhibiting Ac-utilizing ACB, which rely on H_2-utilizing MET to maintain low enough H_2 concentrations to allow thermodynamically spontaneous reverse acetogenesis. The pore water Ac is subsequently metabolized by Ac-utilizing MET, with the upshot that acSR is decreased. The removal of Ac seems to be a more important secondary control on AOM than the higher pore water H_2 concentrations resulting from increased fs^{H2}_{MET}.

Finally, fs^{CH4H2O}_{MOA} lies on the right-hand-side of the normal distribution curve. Because of the stoichiometric coefficient for H_2 of $2fe/fs$ in the macrochemical equation for AOM (R_{11m}, table 3), higher *fs* for AOM necessarily implies a lower *fe* (Appendix 1), and thus less H_2 is produced per C mol MOA synthesized. Again, this means that more SO_4^{2-} is available for oxidation pathways. Although CH_4 consumption from the pore water is also lower due to higher fs^{CH4H2O}_{MOA}, this has no effect on AOM rates, because MOA are not kinetically inhibited by the CH_4 concentration; F_K for AOM is always around 0.5 (fig. 3H).

In summary, the sensitivity of the rate of AOM on the *fs* parameters arises from the dynamic interplay of H_2 and Ac in the system, and not from biomass growth. Hence, the simple view that higher substrate turnover rates correlate with higher total cell numbers may not be true in complex geomicrobial reaction systems characterized by intensive substrate competition. The low F_{TOT} values for all pathways in the reaction network (fig. 3J) imply that cellular activities and growth of biomasses are severely limited. The values of *fs* impact cellular activities by regulating the consumption and production of reactive intermediates (Ac and H_2).

Thermodynamic parameters.—Of the average stoichiometric numbers (χ, Appendix 4), χ^{H2}_{SRB} and χ^{Ac}_{MET} are the most sensitive ones (fig. 5). The significant departure of χ^{CH4H2O}_{MOA} from the normal distribution further confirms that thermodynamic constraints exert a major control on AOM rates (Hoehler and others, 1994): χ^{CH4H2O}_{MOA} is positioned to the left of the line, because increasing this parameter reduces the

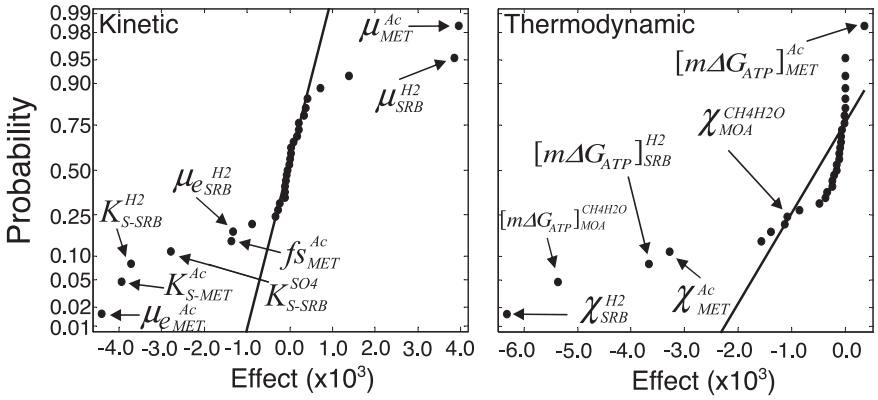

Fig. 6. Normal probability plots for the most sensitive kinetic and thermodynamic parameters determined from figure 5. See text for complete discussion.

effective Gibbs energy yield ΔG_{NET} / χRT (eq A-20). Values of χ are estimated from the number of times the rate-determining step occurs in the electron transport chain (Jin and Bethke, 2002), which can be associated with proton translocation across the cell membrane (Jin and Bethke, 2005). Nonetheless, χ is poorly known for the microbial pathways included in the reaction network, and a value of χ=1 per electron transferred via catabolism has been used in this model, based on the work on anaerobic respiration of Jin and Bethke (2005) (Appendix 4).

The values of $[m\Delta G_{ATP}]^{CH4H2O}_{MOA}$ and $[m\Delta G_{ATP}]^{H2}_{SRB}$ are by far the most sensitive threshold parameters, because hySR coupled to AOM are pathways which function at their bioenergetic edge (Hoehler and others, 1994). The star on figure 5 represents the interaction of $[m\Delta G_{ATP}]^{CH4H2O}_{MOA}$ and $[m\Delta G_{ATP}]^{H2}_{SRB}$, further emphasizing that AOM strongly depends on SRB to lower the H_2 concentration (Hoehler and others, 1994). In nature, the structural arrangement of SRB-MOA aggregates, consisting of an inner core of MOA surrounded by an outer shell of SRB, may be an evolutionary adaptation to maximize the thermodynamic efficiency of AOM (Boetius and others, 2000; Knittel and others, 2003).

Key parameters and processes.—For each individual parameter type in figure 5, the most sensitive parameters are selected and grouped into those affecting kinetic and thermodynamic driving forces, respectively. Two additional fractional factorial analyses then help identify those parameters that most strongly affect the model output (fig. 6). For the kinetic parameters, it appears that uncertainty in modeled AOM rates arises primarily from the parameterization of the rates of the acME and hySR processes, hence demonstrating that SRB and MET are key organisms controlling CH_4 turnover in coastal marine sediments. Again, it should be noted that the AOM rate is much less sensitive to the actual values assigned to the kinetic parameters of the AOM process itself.

The key roles played by SRB and MET are also apparent from the sensitivity analysis of the thermodynamic parameters. However, in addition, the threshold Gibbs energy for ATP synthesis ($m\Delta G_{ATP}$) for methane oxidation has a major effect on the rate of AOM. This is not entirely surprising given that MOA are functioning close to their bioenergetic limit. Caution must be exerted in interpreting the results of figure 6, because the same values of χ and $m\Delta G_{ATP}$ are assigned to all pathways in the baseline simulation (table 4). This need not be the case (Jakobsen and Postma, 1999; Hoehler and others, 2001; Thornton and others, 2001), and may effect the relative positions of

the predicted effects on the probability plots. Nonetheless, the analysis presented here implies that better estimates of χ, particularly for hySR and acME, and $m\Delta G_{ATP}$, particularly for hySR, acME and AOM, would benefit the quantitative prediction of CH_4 dynamics in coastal sediments.

Methane Turnover in Coastal Marine Sediments

Kinetic and thermodynamic controls on AOM.—Temperature plays an important role in the kinetics of enzymatically-mediated reactions in nearshore marine environments. Microorganisms in coastal sediments tend to be psychrophilic or mesophilic, meaning that a temperature increase between 278K and 288K will lead to an increase in growth rates and metabolic activity. In the model, temperature affects the values of μ *and* μ_e (table 4) through the imposed Q_{10} value (fig. 1), but also the values of $\Delta G^{o'}$ through the van't Hoff Equation (Appendix 4).

To isolate the direct role of temperature, the baseline simulation is compared to simulations where temperature is held constant. The temporal trends of the rates of hySR and AOM computed at two constant temperatures (278K and 288K) are generally similar to those obtained in the baseline simulation (fig. 7). As expected, the maximum rates are smaller in the lower temperature simulation. However, the integrated rate of AOM varies marginally, from 51.9 nmol cm^{-3} a^{-1} (278K) to 66.0 nmol cm^{-3} a^{-1} (288K), compared to the baseline simulation value of 59.8 nmol cm^{-3} a^{-1}. The most obvious effect of variable temperature in the baseline simulation is the shift toward late winter of the maximum hySR and AOM rates and the asymmetry in the rate profiles. Because the maximum specific growth rate, μ, for hySR changes with temperature, the substrate affinity (μ/K_S) is also temperature-dependent, which results in the asymmetric hySR and AOM peaks. In contrast, at constant temperature, substrate affinities (μ/K_S) remain constant, which means that the variability in process rates at 278K and 288K are solely driven by F_T and F_K. Although the baseline and constant temperature simulations are clearly different, the simulation results agree with experimental results, whereby PCS reactivity (Westrich and Berner, 1984, 1988) and SO_4^{2-} input (Hoehler and others, 1994), rather than temperature, are the principal factors driving the seasonal variability in CH_4 turnover in shallow-water sediments.

The concentration of SO_4^{2-} is the most important variable determining the fate of fermentation products (H_2, Ac). In winter, H_2 and Ac are mostly oxidized by SO_4^{2-} (figs. 3D and 3F), whereas in summer they are important substrates for methanogenesis. Competitive exclusion of MET by SRB for H_2 and Ac is well-documented (Lovley and others, 1982; Lovley and Goodwin, 1988; Jakobsen and Postma, 1999), although in environments with very high rates of sulfate reduction (~2400 nmol cm^{-3} d^{-1}; Holmer and Kristensen, 1994) sulfate reduction and methanogenesis may occur simultaneously because of abundant Ac and H_2. Apparent inhibition of MET is not due to the presence of SO_4^{2-} *per se*, but rather to the reduction in H_2 concentration engendered by the higher affinity of the SRB for H_2: in the model, the affinity (μ/K_S) of MET for H_2 at 278K (table 4) is two orders of magnitude lower than that for SRB.

The half-saturation constant, K_S, for H_2 uptake by MET (1000 nM) and, especially for SRB (10 nM), used in the baseline simulation are significantly lower than some values obtained in culture experiments (Kristjansson and others, 1982; Robinson and Tiedje, 1984). The latter values, typically in the μM range, have been questioned (Lovley and Chapelle, 1995). In particular, Giraldo-Gomez and others (1992) propose that mass transfer limitations in culture experiments may result in apparent K_S values for H_2 that are orders of magnitude too high. In support of this view, when K_{S-SRB}^{H2} in the range 1 to 10 μM are imposed for hySR in the simulations, the H_2 concentration remains systematically too high for AOM to take place. With the baseline K_S values for

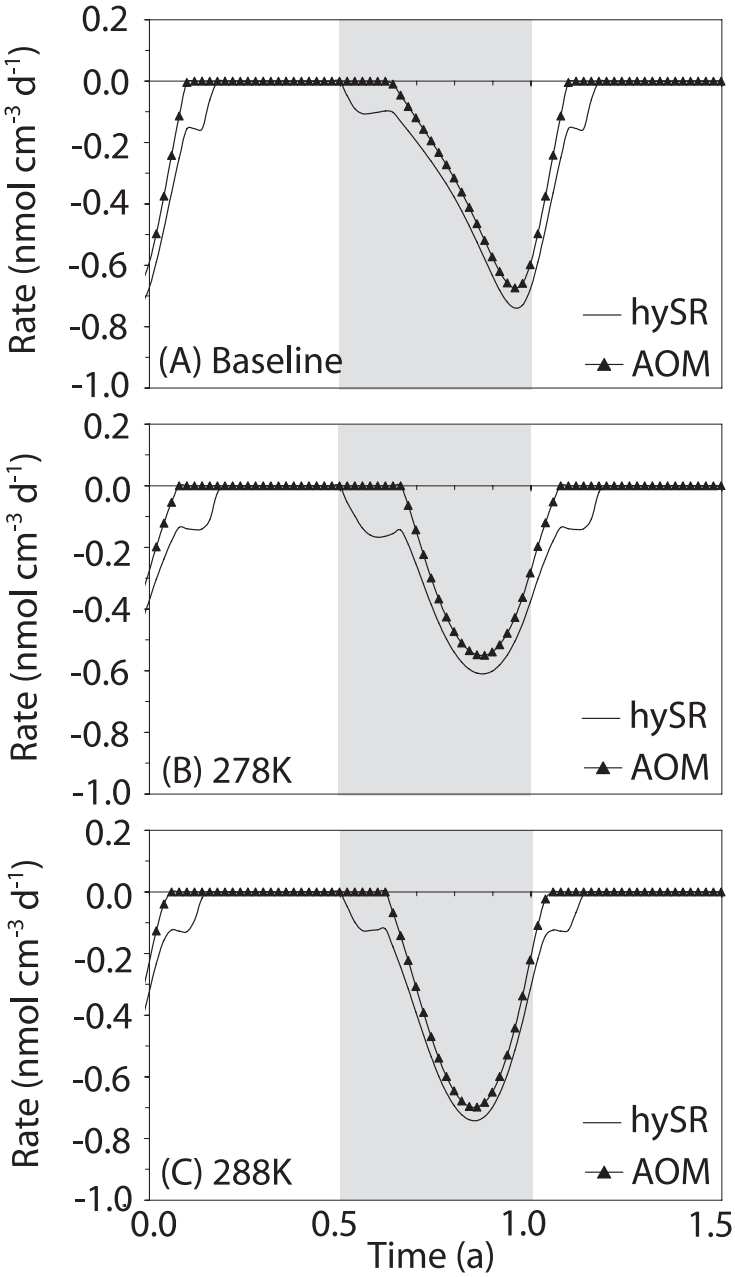

Fig. 7. Comparison of the baseline simulation (A) and two simulations at constant temperatures of (B) 278K and (C) 288K, respectively. Note that in the baseline simulation the temperature varies seasonally (fig. 1). Key: hySR = hydrogenotrophic sulfate reduction (R_{7m}, nmol SO_4^{2-} cm^{-3} d^{-1}), AOM = anaerobic methane oxidation (R_{11m}, nmol CH_4 cm^{-3} d^{-1}). The winter period is indicated by the shading.

H_2 uptake, however, the modeled H_2 concentrations during winter (0.44 nM) and summer (7.5 nM) are in good agreement with field H_2 concentrations reported for aquatic sediments dominated by coupled AOM-SR and methanogenesis, respectively (Lovley and Goodwin, 1988; Hoehler and others, 1994).

AOM is mainly thermodynamically driven (fig. 3G). Initiation of AOM occurs when H_2 concentrations fall below approximately 0.5 nM, which compares favorably with the 0.16 nM reported for Cape Lookout Bight (Hoehler and others, 1994). Thus, the Gibbs energy yield for AOM (ΔG_{NET}, eq A-18) acts as the switch which opens or closes the window-of-opportunity for AOM. In turn, ΔG_{NET} is very sensitive to the H_2 concentration and to the threshold Gibbs energy for ATP synthesis ($m\Delta G_{ATP}$, eq A-18), which is set here to 4.0 kJ (mol CH_4)$^{-1}$. The imposed value is lower than the minimum catabolic Gibbs energy yield for ATP synthesis often quoted in the literature (15 – 20 kJ mol^{-1}, see Appendix 4). Yet, additional numerical experiments (not shown) revealed that AOM was thermodynamically inhibited using the literature threshold values; the process being only possible below a threshold limit of 10.0 kJ (mol CH_4)$^{-1}$. The latter is an optimum threshold value, applicable only if all dispersed cells are in direct contact with the bulk solution. The current model makes no account of microchemical diffusion of the reactive intermediates within SRB-MOA aggregates, a process which consumes a fraction of the Gibbs energy (Dolfing, 1992; Sørensen and others, 2001). Nonetheless, Jackson and McInerney (2002) observed that microbial metabolism in syntrophic associations can proceed close to thermodynamic equilibrium. This suggests that some microorganisms possess energy conservation mechanisms which permit net synthesis of a molecule of ATP from several revolutions of the catabolic cycle. The energy conservation pathway in MOA is as yet unknown, but from the low Gibbs energy yields for AOM observed in the field (for example, Boetius and others, 2000; Bian and others, 2001) it appears likely that similar mechanisms allow MOA to metabolize at energy yields significantly lower than 15 to 20 kJ mol^{-1}.

The kinetic drive for AOM is always high (F_K, fig. 3H). The CH_4 half-saturation constant for AOM (K_{S-MOA}^{CH4H2O}) is assumed to be equal to 1.5 mM (table 4). Actual values of K_{S-MOA}^{CH4H2O} are not well constrained, although sediment incubation experiments by Nauhaus and others (2002) suggest values $\geq$ 10 mM for AOM microbes from CH_4 seeps. Model simulations (not shown) with K_{S-MOA}^{CH4H2O} ranging from 0.1 to 10 mM result in annual integrated AOM rates of 60.1 nmol cm^{-3} a^{-1} (0.1 mM) to 56.3 nmol cm^{-3} a^{-1} (10 mM), compared to the baseline simulation value of 59.8 nmol cm^{-3} a^{-1}. These relatively small changes are consistent with the results of the global sensitivity analysis which show that the rate of AOM is not very sensitive to the kinetic parameters of AOM. Furthermore, from the stoichiometry of the reaction (table 2), AOM cannot exceed ¼ of the rate of diffusive H_2 transport away from the MOA. Therefore, CH_4 would only become truly limiting in the window-of-observation when the extracellular CH_4 concentration of methane drops to levels on the same order of magnitude as those of H_2 (nM); a situation which does not arise in the simulations.

Implications for AOM modeling in coastal marine sediments.—The preponderance of thermodynamic, rather than kinetic, controls on AOM rates under transient conditions calls into question the ability of the bimolecular rate law (eq 4) to accurately predict AOM rates. To illustrate this point further, figure 8A compares the baseline simulation with a simulation where the rate of AOM is calculated by equation (4), assuming a second-order rate constant k_{AOM} of 8000 M^{-1} a^{-1} (Van Cappellen and Wang, 1996). With the exception of AOM, the reaction network is otherwise identical to the bioenergetic model. The time-integrated rate of AOM is 60 percent higher for the bimolecular rate model than for the bioenergetic model. During the time window when AOM occurs, the Gibbs energy yield of AOM in the bioenergetic model is almost constant at the imposed ATP threshold value ($m\Delta G_{ATP}$ = 4.0 kJ (mol reaction)$^{-1}$), and significantly lower than the Gibbs energy yield predicted by the simple kinetic model (fig. 8A). This difference causes a large surplus of methane oxidation in the bimolecular model, especially at the start of winter when AOM is inhibited in the bioenergetic model.

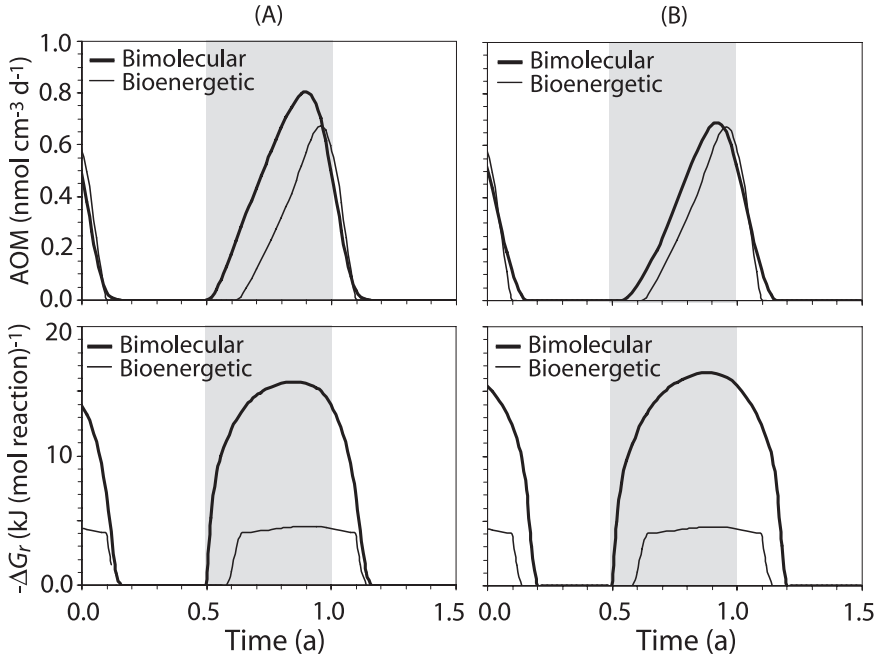

Fig. 8. Rate of AOM (nmol cm^{-3} d^{-1}) and the Gibbs energy yield, $-\Delta G_r$ (kJ mol^{-1}), in the baseline bioenergetic simulation (R_{11m}, table 3), compared to values computed using (A) the simple bimolecular rate expression (eq 4); (B) equation (16), which includes the thermodynamic limitation term. The winter period is indicated by the shading.

When the thermodynamic drive, F_T, is incorporated in equation (4):

$$R_{AOM} = k_{AOM}.F_T.[SO_4^{2-}].[CH_4] \quad (16)$$

the new results are in noticeable closer agreement with those of the bioenergetic model (fig. 8B). Integrated rates using equation (16) are now only 28 percent greater than in the bioenergetic model, while the Gibbs energy yield is essentially unchanged. However, the model continues to predict higher AOM rates because the thermodynamic impact of interspecies competition cannot be captured by equation (16), as it does not explicitly depend on the concentrations of reactive intermediates. At this stage, one may speculate that the relative error associated with the simple bimolecular rate law will tend to be lower in sediments with lower supply of reactive organic substrates and, therefore, lower production of reactive intermediates. Thus, while incorporation of the thermodynamic driving force, F_T, represents a simple improvement of the bimolecular rate equation for AOM, it may still over-predict the time and depth window in which AOM will take place.

Importance of reactive intermediates.—The sensitivity analysis reveals that correct parameterization of acME is crucial for predicting rates of AOM in coastal sediments. Intriguingly, acetotrophy by ACB is also a sensitive process (fig. 5), albeit to a lesser degree, since Ac consumption by acetotrophy is an order of magnitude lower than acME in winter (fig. 4A). To understand why AOM rates are highly dependent on MET, the ecological function of methanogens must be considered. Firstly, one may hypothesize that the principal role of MET in the window-of-observation is to supply CH_4. Secondly, based on the results of the global sensitivity analysis, one may speculate that MET are able to reduce the competition by SRB for reactive intermediates.

The rationale behind the first hypothesis is obvious; without CH_4, MOA cannot thrive because all CH_4 in the model is generated internally. To test this argument, the model was modified by assuming a large influx of CH_4 to the depth interval of interest, in such a way that the dissolved CH_4 concentration is always maintained at the *in situ* solubility (~5 mM). Repeating the sensitivity analysis under these conditions, we observed negligible change in the significance of MET in promoting AOM, which corroborates the low sensitivity of K_{S-MOA}^{CH4H2O} in the global sensitivity analysis. Production of CH_4 by methanogens in the modeled sediment interval is thus of relatively minor importance compared to some other role played by these microorganisms.

With regard to the second hypothesis, acME serves two purposes. First, Ac is directly metabolizable by the SRB, and removal of Ac by methanogenesis therefore diverts more SO_4^{2-} to H_2 oxidation, thereby promoting AOM. Second, acME reduces the rate of acetotrophy and thus H_2 production, which helps to maintain low H_2 concentrations and higher AOM rates. This argument would explain the contrasting sensitivity of acetotrophic MET and ACB (fig. 5).

To validate this latter hypothesis, acME was promoted by lowering K_{S-MET}^{Ac} from 1×10^{-3} to 1×10^{-6} M. The new results are shown in figure 9A, which are compared to the baseline simulation results in figure 9B. The increase in both acME and hySR in winter, compared to the baseline simulation, is clearly evident. The integrated AOM rate has increased from the baseline simulation value of 59.8 to 101.9 nmol CH_4 cm^{-3}, with maximum rates reaching 1.0 nmol CH_4 cm^{-3} d^{-1}, compared to 0.67 nmol CH_4 cm^{-3} d^{-1} in the baseline simulation. Repeating the calculations described earlier for the H_2 seasonal mass balance (fig. 4), indicates that AOM now accounts for 76.0 percent of total SR, compared to only 44.3 percent in the baseline simulation. The contribution from acetotrophy to total SR is negligible. The fraction of total SR due to AOM (fig. 9B) is now $>$ 80 percent for most of the winter period, and reaches a maximum of 91 percent. All other things being equal, enhanced acME has a large effect on the proportion of CH_4 oxidized to H_2 to meet SRB electron demand, despite the fact that only 24 percent of total acME occurs during winter concomitant with H_2 consumption by SRB (fig. 4A). This is because the low half-saturation constant for Ac decreases the mean year-round Ac concentration (fig. 9A) and, in turn, prevents its use as a sink for SO_4^{2-} when produced during winter.

Furthermore, acME removes Ac from the system and marginalizes ACB by inhibiting acetotrophic degradation. To a certain extent, this argument depends on the ability of ACB found in natural environments to operate in reverse, in syntrophic partnership with a methanogen (Sansone and Martens, 1982; Lee and Zinder, 1988; Nüsslein and others, 2001). However, even by removing the reversibility of ACB, we arrive at the same conclusion; that is, non-AOM-derived reactive intermediates which supply SRB with electron equivalents are the overriding control of AOM rates on the bulk pore water scale of the model. Higher proportions of noncompetitive substrates for methanogenesis in marine environments, such as formate, methanol and methylamines which are not used by SRB (Oremland and Polcin, 1982; King, 1984; Ferdelman and others, 1997) would tend to reduce the impact of MET on AOM.

The role of indirect substrate competition has been recognized for many years, although not in the context of AOM. In organic-rich marine sediments, where SO_4^{2-} concentrations rapidly drop to low levels below the sediment-water interface, Ac is a significant CH_4 precursor and causes competition between SRB and MET (Senior and others, 1982; Crill and Martens, 1986). Additionally, acetogenic microorganisms can affect the terminal steps of carbon flow in anaerobic environments through substrate competition (for H_2) and production (for Ac) (Dolfing, 1988; Ferdelman and others, 1997). As Avery and others (2002) observed, understanding the competition and

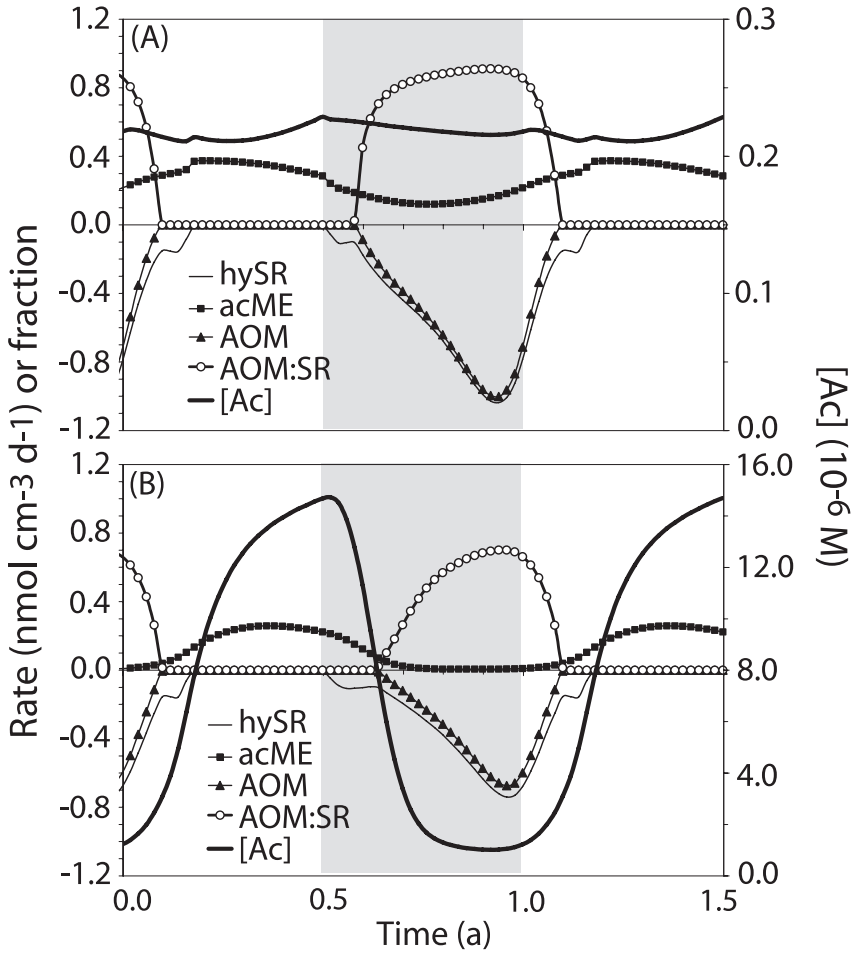

Fig. 9. Simulation results using (A) parameter values listed in table 4 (the baseline simulation) with the exception of K_{S-MET}^{Ac} which is reduced from 1×10^{-3} to 1×10^{-6} M, compared with (B) the baseline simulation. Positive process rates indicate production and negative rates indicate consumption. Key: hySR = hydrogenotrophic sulfate reduction (R_{7m}, nmol SO_4^{2-} cm^{-3} d^{-1}), acME = acetotrophic methanogenesis (R_{10m}, nmol CH_4 cm^{-3} d^{-1}), AOM = anaerobic methane oxidation (R_{11m}, nmol CH_4 cm^{-3} d^{-1}), AOM:SR = the fraction of total SR due to AOM. The winter period is indicated by the shading.

inhibition of microbially-mediated processes is crucial to predict controls on substrate turnover and chemical fluxes.

Accordingly, the maximum potential impact of competing microbial processes on AOM can be roughly quantified by considering the relative importance of each assimilative pathway in terms of production or consumption of H_2 and Ac. For example, the annual integrated rate of Ac consumption by acME is 40.3 nmol Ac cm^{-3} a^{-1}. From the SO_4^{2-}:Ac stoichiometry of 1:1.08 in acSR (R_{9m}, table 3), this rate of Ac consumption by acME represents a saving of 37.3 nmol SO_4^{2-} cm^{-3} a^{-1}. If this SO_4^{2-} were re-invested in hySR, a total of 157.2 nmol H_2 cm^{-3} a^{-1} could be oxidized via this pathway, because the stoichiometry of SO_4^{2-}:H_2 (R_{7m}, table 3) is 4.21. Thus, on an annual basis, if 3.86 mol H_2 are released per CH_4 oxidized (R_{12m}, table 3), then each 40.3 nmol Ac cm^{-3} degraded via acetotrophic methanogens favors the anaerobic

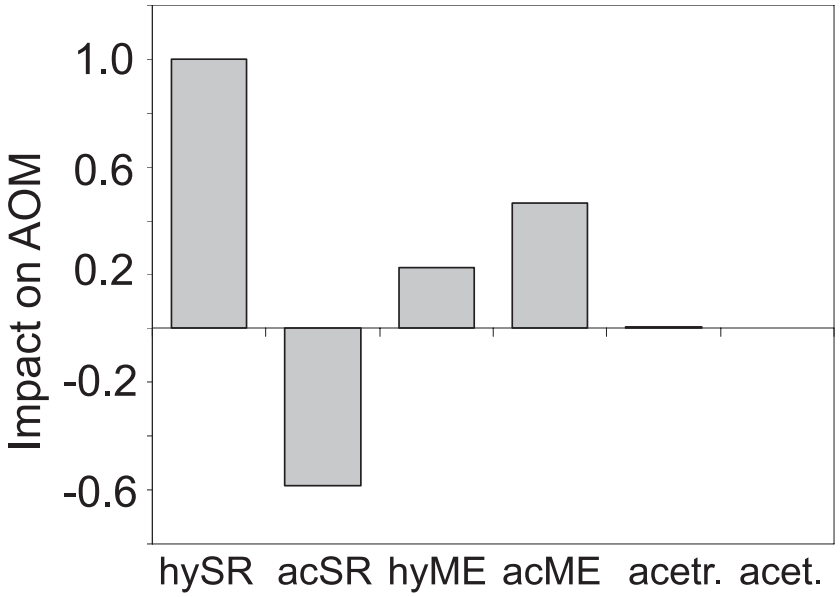

Fig. 10. Potential impact of the various pathways in the reaction network on the rate of AOM, normalized to the rate of hydrogenotrophic sulfate reduction (see text for detailed explanation). Key: hySR = hydrogenotrophic sulfate reduction (R_{7m}, table 3), acSR = acetotrophic sulfate reduction (R_{8m}), hyME = hydrogenotrophic methanogenesis (R_{9m}), acME = acetotrophic methanogenesis (R_{10m}), acetr. = acetotrophy (R_{14m}), acet. = acetogenesis (R_{13m}).

oxidation of a maximum of (157.2/3.86=) 40.7 nmol CH_4 cm^{-3}, that is, each mol Ac fermented to methane favors the loss of 1.01 mol CH_4 cm^{-3} via AOM.

The same calculation can be repeated for the various reaction pathways, in order to compare the relative impact of each process on AOM. The results are shown in figure 10, where potential rates of CH_4 consumption are normalized to that of hySR — the most influential process on AOM. These results are interesting in many ways. For instance, acSR has the largest impact on the rate of AOM, and the impact is negative because acSR consumes SO_4^{2-}, which could otherwise be invested in coupled hySR-AOM. The figure shows that 58 percent more AOM would be possible if the SO_4^{2-} channeled into acSR is instead used for hySR. The acME and hyME pathways account for 46 percent and 23 percent of the effect of hySR, respectively, and have positive impacts, meaning that these pathways promote AOM. These large contributions are surprising, especially considering that methanogens play no direct role in coupled hySR-AOM. Therefore, from the viewpoint of methane oxidation, a significant fraction of SO_4^{2-}, which could otherwise be invested in AOM, is lost to acSR; acME (and hyME) effectively removes a competing substrate from utilization by SRB, allowing more SO_4^{2-} to be channeled into hySR, thereby promoting AOM and extending the season of MOA activity, as observed in figure 9. Even though we have assumed that fermentation produces H_2 and Ac only, we believe that the conclusions apply to all labile reactive intermediate substrates used by both SRB and MET, although their applicability depends on the capacity of spatially organized consortia of SRB-MOA to assimilate substrates at the same rate as single, dispersed cells (Nauhaus and others, 2005). The result in figure 10 also implies that ACB have very little effect on AOM. This is consistent with the fact that acetogenesis produces Ac and consumes H_2, and vice-versa for acetotrophy. Competition between MET and ACB for Ac will determine how much

carbon is effectively made unavailable to the ACB (via CH_4 production) and how much is recycled internally (via acetogenesis and acetotrophy).

The arguments presented above actually help explain the variation in the fraction of SR coupled to AOM in coastal marine sediments. For example, this fraction is estimated at 8 to 20 percent in Eckernförde Bay (Bussmann and others, 1999; Treude and others, 2005), 50 percent in Århus Bay (Thomsen and others, 2001), <0.1 percent in Kysing Fjord (Ivsersen and Blackburn, 1981), 5 to 20 percent in Skan Bay (Reeburgh, 1980) and 23 to 40 percent in Saanich Inlet (Devol and others, 1984). The depth of the SMTZ in these areas is generally less than 1.5 m below the sediment surface, because of relatively high organic matter deposition fluxes. In contrast, in continental slope sediments, which receive lower organic matter inputs, fractions of 11 to 100 percent for the Namibian shelf have been reported (Niewöhner and others, 1998; Fossing and others, 2000), 50 to 100 percent for Amazon Fan sediments (Burns, 1998; Adler and others, 2000) and >80 percent for the Japan Sea and Peru Margin sediments (D'Hondt and others, 2002). Here the SMTZ is generally deeper than in nearshore sediments and diffusive SO_4^{2-} supply to the SMTZ constitutes an important sink for CH_4 (but see Discussion in Jørgensen and others, 2001). In contrast, in areas of active fluid venting where the SMTZ is located a few cm below the sediment surface, the contribution of AOM to total SR is highly variable (Treude and others, 2003; Joye and others, 2004; Kallmeyer and Boetius, 2004), and in some cases methane may only play a secondary role as terminal electron donor compared to non-methane hydrocarbons (Formolo and others, 2004). Whereas the fraction of SR due to AOM has previously been explained on the basis of carbon substrate availability for SRB, the model developed here shows that high concentrations of reactive carbon substrate may lead to thermodynamic and kinetic inhibition of AOM through interspecies competition for reactive intermediates.

SUMMARY AND CONCLUSIONS

Anaerobic oxidation of methane (AOM) is a key process preventing methane generated in marine sediments from escaping to the water column and, eventually, to the atmosphere. The efficient capture of methane by AOM at the global scale contrasts with the low energetic yields of this process and the sluggish growth rates of the methane oxidizing microbial communities. In this paper a batch modeling approach is used to gain a better understanding of the environmental, physiological and ecological controls on AOM activity in coastal marine sediments, where methanogenesis occurs in fairly close proximity to the sediment-water interface.

The environmental forcings on the microbial reaction network producing and consuming methane are the seasonal cycle of temperature and those of sulfate and organic matter input to the sulfate-methane transition zone. These forcings create seasonal variations in the local concentrations of pore water constituents that modulate the ecological interactions between the microbial groups considered in the model: sulfate reducers, methanogens, methane oxidizers, acetogens and fermenters. The model explicitly accounts for the production and consumption of the reactive intermediates, H_2 and acetate, as well as for growth and decay of the functional microbial groups involved.

Synthesis of new biomass occurs through the coupling of catabolic and anabolic half-reactions, which leads to a macrochemical equation specific to each energy yielding pathway. The macrochemical equation expresses the stoichiometry of constituent consumption and production per unit biomass produced. Anabolism is either autotrophic or heterotrophic, depending on the source of the electrons used for cell synthesis. The partitioning of electrons between energy generation and growth is governed by the growth yield, which is calculated from the Gibbs energy cost of biomass synthesis, following Rittmann and McCarthy (2001). Maximum specific growth

and relative decay rates are similarly obtained from thermodynamic considerations, the former from the maximum rate of substrate utilization and the latter from the standard Gibbs energy change of the macrochemical growth equation. The approach presented thus provides a general framework for the systematic derivation of key microbial growth parameters.

Because AOM activity in marine sediments is operating close to the bioenergetic limit, the model also considers the possible thermodynamic limitation of growth of the microbial groups (Jin and Bethke, 2002). This is achieved by including thermodynamic functions in the classical Michaelis-Menten kinetic model for substrate uptake, which slow down anabolism as the Gibbs energy yield of catabolism approaches the minimum requirement for ATP synthesis. The differential equations describing growth of the various microbial groups are then solved to yield the seasonal changes in biomasses, pore water chemistry and reaction rates within a fixed depth interval (the "window-of-observation") of a shallow-water, anoxic marine sediment in a temperate climate setting.

While the seasonally forced supply of sulfate and labile organic compounds to the window-of-observation engender major seasonal shifts in the redox state and microbial reaction dynamics, the biomasses of the various functional groups of microorganisms show relatively small changes on a seasonal time scale. In other words, the microbial reaction dynamics are dominated by fluctuations in cellular activity levels of the microorganisms, rather than by fluctuations of their abundances. The seasonal temperature variability causes a time lag in the supply and uptake of the major substrates, but plays a relatively minor direct role in the seasonal variability in AOM activity, because biomass growth is to a large extent limited by substrate availability and by bioenergetic constraints.

The activities of methanogens and sulfate reducers are determining for the annual rate of AOM within the sediment depth interval considered. The role of methanogens is not limited to the production of methane, however. By removing acetate from the pore waters, acetotrophic methanogens also promote the oxidation of H_2 coupled to sulfate reduction. The resulting drop in H_2 concentration then allows AOM to become thermodynamically spontaneous. The efficient anaerobic oxidation of methane therefore relies on the presence of a sufficiently high biomass of methane oxidizers that are able to rapidly respond to the changing H_2 levels.

A global sensitivity analysis of the model, based on a factorial design, confirms that the most sensitive kinetic and growth-related parameters influencing the (annual) rate of AOM are those corresponding to hydrogenotrophic sulfate reduction and acetotrophic methanogenesis. However, under the seasonally-transient conditions encountered in nearshore marine sediments, the kinetic parameters describing substrate uptake and biomass growth of the methane oxidizing archaea themselves are not very sensitive. That is, the rate of AOM is mainly controlled by the production and consumption of intermediate energy substrates such as H_2 and acetate. The sensitivity analysis further identifies the threshold for ATP energy conservation in AOM as a key parameter, because it also determines when methane oxidation becomes thermodynamically feasible.

As emphasized in previous work, anaerobic methane oxidation is a marginal energy yielding process. In anoxic nearshore sediments that are not associated with methane seeps, the activity of the methane oxidizers is therefore mainly regulated by the activities of other members of the resident microbial community, which rely on more efficient catabolic pathways. AOM in these environments can thus only be properly understood by considering the entire network of geomicrobial reactions producing and consuming methane. Furthermore, as shown here, this reaction network is constrained by both kinetic and thermodynamic limitations on the various

metabolic pathways. The logical next step will be to incorporate the reaction network into a reactive transport model, in order to determine how physical transport processes affect the functioning of the AOM reaction network in different sedimentary environments.

ACKNOWLEDGMENTS

The authors acknowledge the generous and invaluable guidance of Bruce Rittmann for the derivation of microbial growth parameters, as well as the constructive comments of Jeanne VanBriesen. We thank Yvonne van Lith for assistance with the factorial design. The manuscript has benefited from the instructive comments of two anonymous reviewers. This work is financially supported by EU-project METROL (contract no. EVK3-CT-2002-00080), and the Netherlands Organization for Scientific Research (NWO Pioneer Programme).

APPENDICES

In the Appendices, semi-empirical expressions to calculate microbial growth parameters are presented. Where possible, these expressions are used, rather than relying on parameters derived from highly specific laboratory studies, such as pure culture experiments, or model-fitted parameters from the literature. Figure A-1, which schematically shows the model structure, complements the Appendices.

Appendix 1. Cellular Growth Yields

The methodology of Rittmann and McCarty (2001), applied by Rittmann and VanBriesen (1996) and Yuan and VanBriesen (2002), is followed. In microbial growth, electrons from the electron donor (E_D) are proportioned into anabolism, to synthesize biomass, and catabolism, to generate energy. If $\Delta G^{o\prime\prime}$ is the standard Gibbs energy of catabolism, expressed per electron equivalent (kJ e-eq^{-1}), at neutral pH and 298K (see table 2), and $\Delta G^{o'}_{syn}$ is the standard Gibbs energy of (anabolic) cell synthesis (kJ e-eq^{-1}), under the same conditions, then the energy and electron balances can be expressed as (VanBriesen, 2002):

$$-feK\Delta G^{o'} = fs\Delta G^{o'}_{syn} \tag{A-1}$$

with

$$fe + fs = 1 \tag{A-2}$$

where *fe* is the fraction of electrons transferred from the E_D to the terminal electron acceptor (E_A) (e-eq (e-eq E_D)$^{-1}$), and *fs* is the fraction of E_D electrons invested in biomass production (e-eq cells (e-eq E_D)$^{-1}$); *K* is the efficiency of catabolic energy capture, which is assigned an average value of 0.6 (60%). The remaining 40 percent of energy is dissipated as heat; it reflects the net entropy generation within the cell as a result of the irreversible nature of growth (Rittmann and McCarty, 2001; VanBriesen, 2002).

The energy cost of biomass synthesis, $\Delta G^{o'}_{syn}$, is calculated assuming that pyruvate (CH_3COCOO^-) is a representative cellular intermediate for biomass synthesis [external carbon source → pyruvate → biomass]. Thus:

$$\Delta G^{o'}_{syn} = \frac{(\Delta G^{o'}_{pyr} - \Delta G^{o'}_{ED})}{\epsilon^n} + \frac{\Delta G^{o'}_{cells}}{\epsilon} \tag{A-3}$$

where $\Delta G^{o'}_{pyr}$ and $\Delta G^{o'}_{ED}$ are the standard Gibbs energies of the half-reactions for reduction of pyruvate (35.09 kJ e-eq^{-1} at 298K; Rittmann and McCarty, 2001) and oxidation of the various E_D (table 2), respectively; $\Delta G^{o'}_{cells}$ is the Gibbs energy required to synthesize biomass from pyruvate and equals 18.8 kJ e-eq^{-1} for biomass of composition $C_5H_7O_2N$, at 298K. The efficiency of energy transfer, ϵ, is akin to *K* and taken to be 0.6. The exponent *n* is an integer that accounts for the fact that conversion of the carbon source to pyruvate may release energy for some E_D (for example, glucose, $n = -1$) and consume energy for others (for example, acetate, $n = +1$). For autotrophic reactions, the electron donor is H_2, and an inorganic carbon source is used. This means that, for autotrophic reactions, the $\Delta G^{o'}_{ED}$ values listed in table 2 cannot be used since the E_D contains no carbon to produce pyruvate. For autotrophy, Rittmann and McCarty (2001) therefore propose to set $\Delta G^{o'}_{ED}$ equal to the value of the water-oxygen half-reaction in photosynthesis (-78.2 kJ e-eq^{-1} at 298K) in which organic carbon is synthesized from carbon dioxide. In this case, the value of $\Delta G^{o'}_{pyr} - \Delta G^{o'}_{ED}$ at 298K is

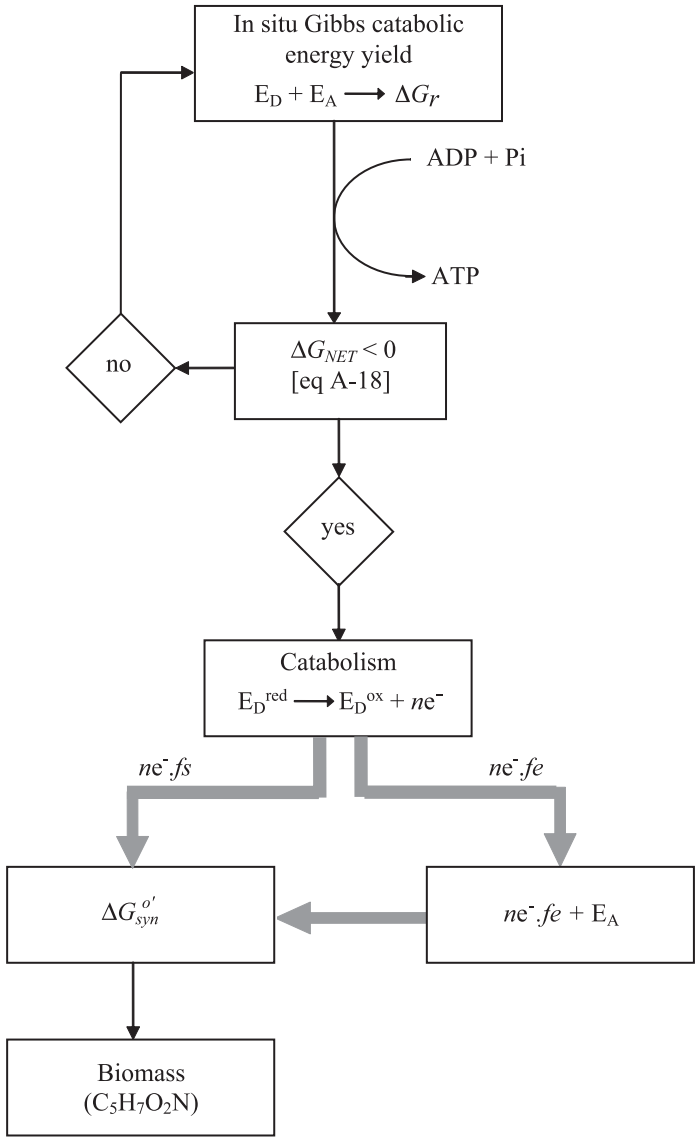

Fig. A-1. Structure of the bioenergetic model. The diagram shows the thermodynamic control on the catabolic process and the partitioning of electrons leading to biomass formation. Catabolism coupling an electron donor (E_D) and acceptor (E_A) will only proceed if the thermodynamic threshold for ATP synthesis is met. Electron flows are denoted by the solid gray arrows.

(35.09-(-78.72)=) 113.8 kJ e-eq^{-1}. Using autotrophic hydrogenotrophic sulfate reduction (R_7, table 2) as an example, equation (A-3) yields (at 298K):

$$\Delta G_{syn}^{o'} = \frac{113.8}{0.6^1} + \frac{18.8}{0.6} = 221.0 \text{ kJ e-eq}^{-1}$$

The relative distribution of electrons over catabolism and anabolism is given, according to equation (A-1), by:

$$A = \frac{fe}{fs} = \frac{-\Delta G^{o'}_{syn}}{K\Delta G^{o'}} \tag{A-4}$$

which, combined with equation (A-2) gives:

$$fs = \frac{1}{1+A} \quad \text{and} \quad fe = \frac{A}{1+A} \tag{A-5}$$

Therefore, cellular yield increases as the catabolic energy increases relative to the energy required for cell synthesis. For hydrogenotrophic sulfate reduction, we obtain:

$$A = \frac{-\Delta G^{o'}_{syn}}{K\Delta G^{o'}} = \frac{-221.0}{0.6 \times (-19.04)} = 19.35 \tag{A-6}$$

such that fs = 0.049 [e-eq cells (e-eq H_2)$^{-1}$] and fe = and 0.951 [e-eq E_A (e-eq H_2)$^{-1}$]. Based on this approach, table 4 lists the values for $fs_i^{E_D}$ (e-eq cells (e-eq E_D)$^{-1}$) for the various microbial groups i (i = SRB, MET, MOA, ACB, FER) and electron donors E_D. As estimates for AOM and acetotrophy (R_{11m} and R_{14m}, table 3), fs are assumed to equal the lowest fs values derived for the other processes. This approximation is necessary as the reactions are exergonic under standard conditions (positive $\Delta G^{o\prime}$). For fermentation, an average cellular yield of 0.18 [e-eq cells (e-eq E_D)$^{-1}$] is imposed, as reported in Pavlostathis and Giraldo-Gomez (1991) and Rittmann and McCarty (2001), in order to account for the variable nature of substrates used by fermenters in nearshore sediments (Arnosti, 2004).

The standard Gibbs energies at 298 K and 1 bar are used to compute the fs values, and no further temperature and pressure corrections are applied. Note that standard Gibbs energies, rather than actual Gibbs energies, are used to calculate growth yields. This uniquely defines the partitioning of electrons for a given electron donor. In biomass implicit models, the values for fs and fe are factored into the term for v_{max} (commonly termed the maximum growth rate), along with the maximum specific growth rate (μ_{max}) and the steady-state biomass concentration. The actual Gibbs energies funneled into growth and maintenance are linked to catabolism through the F_T term (Appendix 4).

The growth yield for each microbial group and E_D, $Y_i^{E_D}$ (g biomass (g E_D)$^{-1}$) can easily be related to the values of $fs_i^{E_D}$ by using the appropriate unit conversion factors. As an example, for hydrogenotrophic sulfate reduction, $Y_i^{E_D}$ can be expressed from $fs_i^{E_D}$ using the unit conversion for biomass ($C_5H_7O_2N$) in terms of electron equivalents (113 g biomass (20 e-eq cells)$^{-1}$):

$$Y^{H2}_{SRB} = 0.049 \frac{\text{e-eq cells}}{\text{e-eq } H_2} \cdot \frac{2 \text{ e-eq } H_2}{2 \text{ g } H_2} \cdot \frac{113 \text{ g biomass}}{20 \text{ e-eq cells}} = 0.28 \text{ g biomass (g } H_2)^{-1}$$

Molar growth yields (mol C mol E_D^{-1}) can also be readily calculated from the stoichiometry of the macrochemical equations given in table 3. For the above example, this corresponds to 0.025 mol C (mol H_2)$^{-1}$. For AOM (R_{11m}, table 3) the yield has been approximated to 0.07 mol C (mol CH_4)$^{-1}$.

Cellular yields for SRB growing on H_2, and MET growing on Ac and H_2, calculated using this "first-principles" approach (table 4) compare favorably with experimentally-derived yields compiled in the review by Oude Elferink and others (1994), and to model parameterizations by Vavilin and others (1997), Segers and Kengen (1998) and Lokshina and Vavilin (1999). Predicted yields for SRB growing on Ac are lower than those reported by Oude Elferink and others (1994), but comparable to the values of Vavilin and others (1997).

Appendix 2. Maximum Specific Growth Rates

Maximum specific growth rates, μ (d^{-1}), can be derived from the maximum specific rate of substrate utilization, q (g E_D (g biomass)$^{-1}$ d^{-1}), and the growth yield (g biomass (g E_D)$^{-1}$), Y:

$$\mu = qY \tag{A-7}$$

where q, Y and μ are specific for the biomass group and electron donor utilized (Rittmann and McCarty, 2001). Substrate utilization is controlled by the flow of electrons to the electron acceptor. The maximum electron flow, q_e, is approximately equal to 1.0 e-eq E_A (g $C_5H_7O_2N$)$^{-1}$ d^{-1}, at 293K (Rittmann and McCarty, 2001). The maximum rate of substrate utilization is then given by:

$$q = \frac{q_e}{fe} \tag{A-8}$$

where the fraction *fe* (see Appendix 1) is expressed in units of e-eq E_A (g biomass)$^{-1}$. As an example, for hydrogenotrophic sulfate reduction, q is given by:

$$q_{SRB}^{H2} = \frac{1.0 \text{ e-eq } E_A \text{ (g } C_5H_7O_2N)^{-1}d^{-1}}{0.951 \text{ e-eq } E_A \text{ (g } H_2)^{-1}} = 1.05 \text{ g } H_2 \text{ (g}C_5H_7O_2N)^{-1}d^{-1} \quad \text{(A-9)}$$

and, therefore, the maximum specific rate for SRB growth on H_2 is

$$\mu_{SRB}^{H2} = 1.05 \frac{\text{g } H_2}{\text{g}C_5H_7O_2N \text{ d}} \cdot 0.28 \frac{\text{g}C_5H_7O_2N}{\text{g } H_2} = 0.29 \text{ d}^{-1}(293K) \quad \text{(A-10)}$$

The maximum growth rates are further corrected for temperature, assuming a Q_{10} value of 2.6. Table 4 lists $\mu_i^{E_D}$ values at 278 K for the metabolic pathways considered in the model. These values are in general agreement with values used in other model studies (Vavilin and others, 1997; Segers and Kengen, 1998) and with experimentally derived values for cold sediments (Knoblauch and Jørgensen, 1999; Knoblauch and others, 1999; Girguis and others, 2005).

Appendix 3. Relative Maximum Specific Decay Rates

Endogenous decay refers to biomass consumption used to generate energy needed to meet homeostatic requirements, such as osmotic regulation, repair plus re-synthesis of macromolecules, and heat loss (Pirt, 1965). Although data on μ_e are available for a wide range of microorganisms, they tend to be highly specific for the experimental conditions under which they were determined. Decay rates depend on the catabolic pathway utilized by the organisms, and are thus specific to the particular electron donor and biomass group considered. Decay rate constants in this work are based on the empirical formula of Tijhuis and others (1993), which depends on the Gibbs energy dissipated during biomass production:

$$\mu_e = \frac{m_E}{-\Delta G_m^{o'} + \gamma_x \Delta G^{o'}} \quad \text{(A-11)}$$

where m_E is the cellular maintenance energy, equal to 28.9 kJ (mol C)$^{-1}$ a^{-1} at 298K (Tijhuis and others, 1993), $\Delta G^{o\prime}$ is the standard Gibbs energy of catabolism per electron equivalent (kJ e-eq^{-1}) at neutral pH conditions (table 2), γ_X is the degree of reductance of carbon in the biomass (4 e-eq (mol C)$^{-1}$ for $C_5H_7O_2N$; Rittmann and McCarty, 2001) and $\Delta G_m^{o\prime}$ represents the standard Gibbs free energy change, in kJ (mol C biomass)$^{-1}$, of the macrochemical reactions R_{7m}-R_{15m} in table 3 (Heijnen and van Dijken, 1992), which combine catabolism plus anabolism. Decayed biomass is recycled immediately to Gibbs energy equivalents of PCS via the reaction:

$$0.2 \text{ } C_5H_7O_2N + 0.6 \text{ } H_2O + 0.2 \text{ } H^+ \rightarrow 0.2 \text{ } NH_4^+ + 0.17 \text{ } C_6H_{12}O_6 \quad \text{(A-12)}$$

Whereas equation (A-11) reproduces endogenous decay rates under controlled conditions in the laboratory experiments reasonably well (Tijhuis and others, 1993), even for anaerobic conditions (Lovley and Klug, 1986; Islam and Singhal, 2002), its extrapolation to the simulated environmental conditions in the window-of-observation yields decay rates that are unreasonably high. A possible explanation for this discrepancy is the restricted (6 months) growth period of microbial biomasses in the model which results from the seasonal forcing functions imposed. The decay rates are thus the least constrained kinetic parameters in the model. Their determination is therefore performed using trial and error simulations to determine the absolute value of the decay rate constant of a single specific process (fermentation at 278 K, Q_{10}=2.6), all other constants being scaled by the use of equation (A-11) until the concentrations of reactive intermediates become sufficient for interspecies substrate competition to take place. Therefore, our approach differs from many other biomass-explicit models since only one decay rate parameter is fitted, while the relative rates are calculated systematically from thermodynamic constraints.

Because AOM and acetotrophy are non-spontaneous under standard conditions, μ_e for these processes are roughly estimated from their maximum specific growth rates, μ, based on a linear regression of μ_e against μ, of the other spontaneous reactions ($\mu_e = 0.0011\mu + 0.090$, r^2=0.43, n=6). This gives a biomass decay rate of 0.11 a^{-1} for the two AOM and acetotrophy pathways.

Appendix 4. Thermodynamic Driving Forces

The catabolic reactions R_7-R_{15} in table 2 are examples of enzymatically-mediated electron transfers between an electron donor, E_D, and acceptor, E_A:

$$xE_D + yE_A \leftrightarrow xE_{D\text{-}ox} + yE_{A\text{-}red} \tag{A-13}$$

where x and y are stoichiometric coefficients. The Gibbs energy change of the above reaction, under non-standard conditions, ΔG_r (kJ mol^{-1}), is given by:

$$\Delta G_r = \Delta G^{o'} + RT\ln\left[\frac{\{E_{D\text{-}ox}\}^x \cdot \{E_{A\text{-}red}\}^y}{\{E_D\}^x \cdot \{E_A\}^y}\right] \tag{A-14}$$

where R and T are the gas constant (8.314 J K^{-1} mol^{-1}) and absolute temperature (K), respectively, { } denotes activities, and $\Delta G^{o'}$ is the standard Gibbs energy of catabolism (kJ mol^{-1}) at 298K, corrected for neutral pH conditions. To convert from concentrations to activities, the activity coefficients listed in the footnote of table 2 are used. Applying equation (A-14) to hydrogenotrophic sulfate reduction as an example leads to:

$$\Delta G_r = \Delta G^{o'} + RT\ln\left[\frac{\{HS^-\}}{\{H_2\}^4 \cdot \{SO_4^{2-}\}}\right] \tag{A-15}$$

Note that (A-15) corresponds to reaction of one mole of SO_4^{2-}, rather than one mole of electrons, that is, $\Delta G^{o'} = -19.04$ (kJ e-eq^{-1}) $\times$ 8 (e-eq (mol SO_4^{2-})$^{-1}$) $= -152.3$ kJ (mol SO_4^{2-})$^{-1}$. Furthermore, the activity of H^+ does not appear in the activity quotient, as the $\Delta G^{o'}$ values given in table 2 are already corrected for neutral pH 7 (Amend and Shock, 2001). Seasonal changes in $\Delta G^{o'}$ due to the imposed $\pm$10°C temperature variations are estimated with the van't Hoff's equation (Thauer and others, 1977; Amend and Shock, 2001). Pressure effects on $\Delta G^{o'}$ are assumed negligible (Amend and Shock, 2001).

Thermodynamic constraints on catabolism are related to the synthesis of the cellular energy carrier adenosine triphosphate (ATP). ATP plays a key role in cellular energetics, by facilitating reactions at physiologically-acceptable substrate concentrations and coupling anabolism to catabolism. ATP is synthesized from adenosine diphosphate (ADP) and inorganic phosphate (P_i):

$$ADP + Pi \leftrightarrow ATP \tag{A-16}$$

Under typical intracellular conditions, ΔG_{ATP} for equation (A-16) is ~60 kJ (mol ADP)$^{-1}$ (Thauer and others, 1977).

The energy for ATP synthesis originates from the cellular proton motive force, created by extruding protons out of the cell membrane during transfer of electrons down the transport chain. Therefore, a finite number of moles m of ATP can be synthesized from n electrons. For instance, for hydrogenotrophic sulfate reduction ($n = 8$):

$$SO_4^{2-} + 4H_2 + m\text{ADP} + m\text{Pi} \rightarrow HS^- + 4H_2O + m\text{ATP} \tag{A-17}$$

Since ΔG_{ATP} is positive, $m\Delta G_{ATP}$ represents the minimum energy yield of the catabolic reaction. At energy yields ($-\Delta G_r$) below $m\Delta G_{ATP}$, the catabolic reaction is thermodynamically inhibited.

In order to estimate $m\Delta G_{ATP}$ it is necessary to know the number of protons translocated per electron transferred. To our knowledge, this information is poorly known for the microbial species under consideration (for example, Müller, 1993; Deppenmeir and others, 1996). However, synthesis of 1 ATP molecule is widely accepted to require translocation of 3 to 4 protons (Thauer and others, 1977; Schink, 1997), implying that $m\Delta G_{ATP}$ is equal to (60/(3-4)=) 15-20 kJ mol^{-1}. This means that in order for ATP synthesis to take place, the catabolic reaction must generate at least 15 to 20 kJ mol^{-1}, which is believed to represent the energy quantum for prokaryotic survival (Schink, 1997). Nevertheless, experimental data suggest that lower Gibbs energy thresholds, between 3 and 10 kJ mol^{-1}, are permissible (Rothfuss and Conrad, 1993; Chin and Conrad, 1995; Schulz and Conrad, 1996; Conrad, 1999; Jackson and McInerney, 2002; Watson and others, 2003), and need not be the same for all microbial species (Jakobsen and Postma, 1999; Hoehler and others, 2001; Thornton and others, 2001). A value of 4.0 kJ per mol^{-1} overall reaction is used in this work for $m\Delta G_{ATP}$, which is toward the lower range of literature threshold values. Further simulations (not shown) reveal that actual value of $[m\Delta G_{ATP}]_{MOA}^{CH4H2O}$ at which the AOM reaction becomes thermodynamically inhibited in the batch model is equal to 10.0 kJ (mol CH_4)$^{-1}$.

Surplus energy above the $m\Delta G_{ATP}$ threshold goes into creating the net thermodynamic energy yield (ΔG_{NET}, kJ mol^{-1}):

$$\Delta G_{NET} = \Delta G_r + m\Delta G_{ATP} \tag{A-18}$$

Substrate utilization is thus possible when $\Delta G_{NET} < 0$.

Thermodynamic constraints *per se* are not sufficient to predict substrate turnover rates, however, as the true kinetic barrier is the activation energy rather than the Gibbs energy of reaction (Boudart, 1976). A thermodynamic driving force, F_T, derived from nonlinear nonequilibrium thermodynamics (Jin and Bethke, 2002) can be applied to enzymatically-mediated substrate utilization:

$$F_{Ti}^{E_D} = 1 - exp\left(\frac{\Delta G_{NET}}{\chi_i^{E_D} RT}\right) \tag{A-19}$$

where χ is the average stoichiometric number (Boudart, 1976). In a microbiological context, χ is the number of protons translocated across the cell membrane per formula reaction of the catabolic process (Jin and Bethke, 2002, 2005). For the catabolic pathways considered, the values of χ are generally poorly known. Following Jin and Bethke (2005), a value of $\chi=1$ for each electron transferred during anaerobic respiration has been selected for the baseline simulation.

References

Adler, M., Hensen, C., Kasten, S., and Schulz, H. D., 2000, Computer simulation of deep sulfate reduction in sediments of the Amazon Fan: International Journal of Earth Sciences, v. 88, p. 641–654.

Alperin, M. J., and Reeburgh, W. S., 1985, Inhibition experiments on anaerobic methane oxidation: Applied Environmental Microbiology, v. 50, p. 940–945.

Alperin, M. J., Blair, N. E., Albert, D. B., Hoehler, T. M., and Martens, C. S., 1992, Factors that control the stable carbon isotopic composition of methane produced in an anoxic marine sediment: Global Biogeochemical Cycles, v. 6, p. 271–291.

Alperin, M. J., Albert, D. B., and Martens, C. S., 1994, Seasonal variations in production and consumption rates of dissolved organic carbon in an organic-rich sediment: Geochimica et Cosmochimica Acta, v. 58, p. 4909–4930.

Amend, J. P., and Shock, E. L., 2001, Energetics of overall metabolic reactions of thermophilic and hyperthermophilic Archaea and Bacteria: FEMS Microbiology Reviews, v. 25, p. 175–243.

Arnosti, C., 2004, Speed bumps and barricades in the carbon cycle: substrate structural effects on carbon cycling: Marine Chemistry, v. 92, p. 263–273.

Arnosti, C., and Holmer, M., 1999, Carbohydrate dynamics and contributions to the carbon budget of an organic-rich coastal sediment: Geochimica et Cosmochimica Acta, v. 63, p. 393–403.

Avery, G. B. J., and Martens, C. S., 1999, Controls on the stable carbon isotopic composition of biogenic methane produced in a tidal freshwater estuarine sediment: Geochimica et Cosmochimica Acta, v. 63, p. 1075–1082.

Avery, G. B. J., Shannon, R. D., White, J. R., Martens, C. S., and Alperin, M. J., 2002, Controls on methane production in a tidal freshwater estuary and a peatland: methane production via acetate fermentation and CO_2 reduction: Biogeochemistry, v. 62, p. 19–37.

Barnes, R. O., and Goldberg, E. D., 1976, Methane production and consumption in anoxic marine sediments: Geology, v. 4, p. 297–300.

Bian, L., Hinrichs, K., Xie, T., Brassell, S., Iversen, N., Fossing, H., Jørgensen, B., and Hayes, J., 2001, Algal and archaeal polyisoprenoids in a recent marine sediment: Molecular isotopic evidence for anaerobic oxidation of methane: Geochemistry, Geophysics, Geosystems, v. 2, doi:10.1029/2000GC000112.

Blair, N. E., and Carter, W. D., Jr., 1992, The carbon isotope biogeochemistry of acetate from a methanogenic marine sediment: Geochimica et Cosmochimica Acta, v. 56, p. 1247–1258.

Boetius, A., Ravenschlag, K., Schubert, C. J., Rickert, D., Widdel, F., Gieseke, A., Amann, R., Jørgensen, B. B., Witte, U., and Pfannkuche, O., 2000, A marine microbial consortium apparently mediating anaerobic oxidation of methane: Nature, v. 407, p. 623–626.

Boudart, M., 1976, Consistency between kinetics and thermodynamics: The Journal of Physical Chemistry, v. 80, p. 2869–2870.

Boudreau, B. P., and Westrich, J. T., 1984, The dependence of bacterial sulfate reduction on sulfate concentration in marine sediments: Geochimica et Cosmochimica Acta, v. 48, p. 2503–2516.

Box, G. E. P., Hunter, W. G., and Hunter, J. S., 1978, Statistics for experimenters. An introduction to design, data analysis and model building: New York, Wiley, 653 p.

Brock, T. D., Madigan, M. T., Martinko, J. M., and Parker, J., 1994, Biology of microorganisms: New Jersey, Prentice Hall, 909 p.

Brüchert, V., and Arnosti, C., 2003, Anaerobic carbon transformation: experimental studies with flow-through cells: Marine Chemistry, v. 80, p. 171–183.

Burdige, D. J., and Gardner, K. G., 1998, Molecular weight distribution of dissolved organic carbon in marine sediment pore waters: Marine Chemistry, v. 62, p. 45–64.

Burdige, D. J., Skoog, A., and Gardner, K., 2000, Dissolved and particulate carbohydrates in contrasting marine sediments: Geochimica et Cosmochimica Acta, v. 64, p. 1029–1041.

Burns, S. J., 1998, Carbon isotopic evidence for coupled sulfate reduction-methane oxidation in Amazon fan sediments: Geochimica et Cosmochimica Acta, v. 62, p. 797–804.

Bussmann, I., Dando, P. R., Niven, S. J., and Suess, E., 1999, Groundwater seepage in the marine environment: role for mass flux and bacterial activity: Marine Ecology Progress Series, v. 178, p. 169–177.

Chidthaisong, A., and Conrad, R., 2000, Turnover of glucose and acetate coupled to reduction of nitrate, ferric iron and sulfate and to methanogenesis in anoxic rice field soil: FEMS Microbiology Ecology, v. 31, p. 73–86.
Chin, K. J., and Conrad, R., 1995, Intermediary metabolism in methanogenic paddy soil and the influence of temperature: FEMS Microbiology Ecology, v. 18, p. 85–102.
Conrad, R., 1999, Contribution of hydrogen to methane production and control of hydrogen concentrations in methanogenic soils and sediments: FEMS Microbiology Ecology, v. 28, p. 193–202.
Cord-Ruwisch, R., Seitz, H. J., and Conrad, R., 1988, The capacity of hydrogentrophic anaerobic bacteria to compete for traces of hydrogen depends on the redox potential of the terminal electron acceptor: Archives of Microbiology, v. 149, p. 350–357.
Crill, P. M., and Martens, C. S., 1986, Methane production from bicarbonate and acetate in an anoxic marine sediment: Geochimica et Cosmochimica Acta, v. 50, p. 2089–2097.
——— 1987, Biogeochemical cycling in an organic-rich coastal marine basin. 6. Temporal and spatial variations in sulfate reduction rates: Geochimica et Cosmochimica Acta, v. 51, p. 1175–1186.
Crozier, T. E., and Yamamoto, S., 1974, Solubility of hydrogen in water, seawater, and NaCl solutions: Journal of Chemical and Engineering Data, v. 19, p. 242–244.
Davis, J. A., Yabusaki, S. B., Steefel, C. I., Zachara, J. M., Curtis, G. P., Redden, G. D., Criscenti, L. J., and Honeyman, B. D., 2004, Assessing conceptual models for subsurface reactive transport of inorganic contaminants: American Geophysical Union, EOS, Transactions, v. 44, p. 449–453.
D'Hondt, S., Rutherford, S., and Spivack, A. J., 2002, Metabolic activity of subsurface life in deep-sea sediments: Science, v. 295, p. 2067–2070.
da Silva, J. E., Pimentel, M. F., da Silva, V. L., Montenegro, M. C. B. S. M., and Araújo, A. N., 2004, Simultaneous determination of pH, chloride and nickel in electroplating baths using sequential injection analysis: Analytica Chimica Acta, v. 506, p. 197–202.
Deppenmeier, U., Müller, V., and Gottschalk, G., 1996, Pathways of energy conservation in methanogenic archaea: Archives of Microbiology, v. 165, p. 149–163.
Devol, A. H., Anderson, J. J., Kuivila, K., and Murray, J. W., 1984, A model for coupled sulphate reduction and methane oxidation in the sediments of Saanich Inlet: Geochimica et Cosmochimica Acta, v. 48, p. 993–1004.
Dickens, G. R., 2003, Rethinking the global carbon cycle with a large, dynamic and microbially mediated gas hydrate capacitor: Earth and Planetary Science Letters, v. 213, p. 169–183.
Dickens G. R., O'Neil, J. R., Rea, D. K., and Owen, R. M., 1995, Dissociation of oceanic methane hydrate as a cause of the carbon-isotope excursion at the end of the Paleocene: Paleoceanography, v. 10, p. 965–971.
Dolfing, J., 1988, Acetogenesis, *in* Zehnder, A. J. B., editor, Biology of anaerobic microorganisms: New York, John Wiley and Sons, p. 417–468.
——— 1992, The energetic consequences of hydrogen gradients in methanogenic ecosystems: FEMS Microbiology Letters, v. 101, p. 183–187.
Drake, H. L., 1994, Acetogenesis, acetogenic bacteria, and the acetyl-CoA "Wood/Ljungdahl" pathway: past and current perspectives, *in* Drake, H. L., editor, Acetogenesis: London, Chapman and Hall, p. 3–60.
Dueri, S., and Therrien, R., 2003, Factors controlling contaminant transport through the flood sediments of the Saguenay Fjord: Numerical sensitivity analysis, *in* Locat, J., Galvez-Cloutier, R., Chaney, R. C., and Demars, K., editors, Contaminated Sediments: Characterization, Evaluation, Mitigation/Restoration, and Management Strategy Performance: West Conshohcoken, Pennsylvania, ASTM International, ASTM Special Technical Publication 1442, p. 167–182.
Ferdelman, T. G., Lee, C., Pantoja, S., Harder, J., Bebout, B. M., and Fossing, H., 1997, Sulfate reduction and methanogenesis in a *Thioploca*-dominated sediment off the coast of Chile: Geochimica et Cosmochimica Acta, v. 61, p. 3065–3079.
Fey, A., Claus, P., and Conrad, R., 2004, Temporal change of 13C-isotope signatures and methanogenic pathways in rice field soil incubated anoxically at different temperatures: Geochimica et Cosmochimica Acta, v. 68, p. 293–306.
Formolo, M. J., Lyons, T. W., Zhang, C., Kelley, C., Sassen, R., Horita, J., and Cole, D. R., 2004, Quantifying carbon sources in the formation of authigenic carbonates at gas hydrate sites in the Gulf of Mexico: Chemical Geology, v. 205, p. 253–264.
Fossing, H., Ferdelman, T. G., and Berg, P., 2000, Sulfate reduction and methane oxidation in continental margin sediments influenced by irrigation (South-East Atlantic off Namibia): Geochimica et Cosmochimica Acta, v. 64, p. 897–910.
Fukuzaki, S., Nishio, N., and Nagai, S., 1990, Kinetics of the methanogenic fermentation of acetate: Applied Environmental Microbiology, v. 56, p. 3158–3163.
Giraldo-Gomez, E., Goodwin, S., and Switzenbaumm, M. S., 1992, Influence of mass-transfer limitations on the half saturation constant for hydrogen uptake in a mixed-culture CH_4-producing enrichment: Biotechnology and Bioengineering, v. 40, p. 768–776.
Girguis, P. R., Cozen, A. E., and DeLong, E. F., 2005, Growth and population dynamics of anaerobic methane-oxidizing archaea and sulfate-reducing bacteria in a continuous-flow bioreactor: Applied and Environmental Microbiology, v. 71, p. 3725–3733.
Haese, R. R., Meile, C., Van Cappellen, P., and De Lange, G. J., 2003, Carbon geochemistry of cold seeps: Methane fluxes and transformation in sediments from Kazan mud volcano, eastern Mediterranean Sea: Earth and Planetary Science Letters, v. 212, p. 361–375.
Haglund, A. L., Lantz, P., Törnblom, E., and Tranvik, L., 2003, Depth distribution of active bacteria and bacterial activity in lake sediment: FEMS Microbiology Ecology, v. 46, p. 31–38.
Hallam, S. J., Putnam, N., Preston, C. M., Detter, J. C., Rokhsar, D., Richardson, P. M., and DeLong, E. F., 2004, Reverse methanogenesis: testing the hypothesis with environmental genomics: Science, v. 305, p. 1457–1462.

Hansen, L. B., Finster, K., Fossing, H., and Iversen, N., 1998, Anaerobic methane oxidation in sulfate depleted sediments: effects of sulfate and molybdate additions: Aquatic Microbial Ecology, v. 14, p. 195–204.

Harder, J., 1997, Species-independent maintenance energy and natural population sizes: FEMS Microbiology Ecology, v. 23, p. 39–44.

Heijnen, J. J., and van Dijken, J. P., 1992, In search of a thermodynamic description of biomass yields for the chemotrophic growth of microorganisms: Biotechnology and Bioengineering, v. 39, p. 833–858.

Heijnen, J. J., van Loosdrecht, M. C. M., and Tijhuis, L., 1993, A black-box mathematical model to calculate autotrophic and heterotrophic biomass yields based on Gibbs energy dissipation: Biotechnology and Bioengineering, v. 40, p. 1139–1154.

Hinrichs, K. U., and Boetius, A., 2002, The anaerobic oxidation of methane: new insights in microbial ecology and biogeochemistry, *in* Wefer, G., Billett, D., Hebbeln, D., Jørgensen, B. B., Schlüter, M., and Van Weering, T., editors, Ocean Margin Systems: Berlin, Heidelberg, Springer-Verlag, p. 457–477.

Hinrichs, K. U., Hayes, J. M., Sylva, S. P., Brewer, P. G., and DeLong, E. F., 1999, Methane-consuming archaebacteria in marine sediments: Nature, v. 398, p. 802–805.

Hoehler, T. M., Alperin, M. J., Albert, D. B., and Martens, C. S., 1994, Field and laboratory studies of methane oxidation in an anoxic marine sediment — evidence for a methanogen-sulfate reducer consortium: Global Biogeochemical Cycles, v. 8, p. 451–463.

——— 1998, Thermodynamic control on hydrogen concentrations in anoxic sediments: Geochimica et Cosmochimica Acta, v. 62, p. 1745–1756.

Hoehler, T. M., Albert, D. B., Alperin, M. J., and Martens, C. S., 1999, Acetogenesis from CO_2 in an anoxic marine sediment: Limnology Oceanography, v. 44, p. 662–667.

Hoehler, T. M., Alperin, M. J., Albert, D. B., and Martens, C. S., 2001, Apparent minimum free energy requirements for methanogenic Archaea and sulfate-reducing bacteria in an anoxic marine sediment: FEMS Microbiology Ecology, v. 38, p. 33–41.

Holmer, M., and Kristensen, E., 1994, Coexistence of sulfate reduction and methane production in an organic-rich sediment: Marine Ecology Progress Series, v. 107, p. 177–184.

Ingvorsen, K., Nielsen, M. Y., and Joulian, C., 2003, Kinetics of bacterial sulfate reduction in an activated sludge plant: FEMS Microbiology Ecology, v. 46, p. 139–137.

Islam, J., and Singhal, N., 2002, A one-dimensional reactive multi-component landfill leachate transport model: Environmental Modelling and Software, v. 17, p. 531–543.

Iversen, N., 1996, Methane oxidation in coastal marine sediments, *in* Murrel, J. C., and Kelly, D. P., editors, Microbiology of atmospheric trace gases; sources, sinks and global change processes: Berlin, Springer-Verlag, p. 51–68.

Iversen, N., and Blackburn, T. H., 1981, Seasonal rates of methane oxidation in anoxic marine sediments: Applied Environmental Microbiology, v. 41, p. 1295–1300.

Iversen, N., and Jørgensen, B. B., 1985, Anaerobic methane oxidation rates at the sulphate-methane transition in marine sediments from Kattegat and Skagerrak (Denmark): Limnology and Oceanography, v. 30, p. 944–955.

Jackson, B. E., and McInerney, M. J., 2002, Anaerobic microbial metabolism can proceed close to thermodynamic limits: Nature, v. 415, p. 454–456.

Jakobsen, R., and Postma, D., 1999, Redox zoning, rates of sulfate reduction and interactions with Fe-reduction and methanogenesis in a shallow sandy aquifer, Rømø, Denmark: Geochimica et Cosmochimica Acta, v. 63, p. 137–151.

Jakobsen, R., Albrechtsen, H. J., Rasmussen, M., Bay, H., Bjerg, P. L., and Christensen, T. H., 1998, H_2 concentrations in a landfill leachate plume (Grindsted, Denmark): In situ energetics of terminal electron acceptor processes: Environmental Science and Technology, v. 32, p. 2142–2148.

Jin, Q., and Bethke, C. M., 2002, Kinetics of electron transfer through the respiratory chain: Biophysical Journal, v. 83, p. 1797–1808.

——— 2005, Predicting the rate of microbial respiration in geochemical environments: Geochimica et Cosmochimica Acta, v. 69, p. 1133–1143.

Jørgensen, B. B., Weber, A., and Zopfi, J., 2001, Sulfate reduction and anaerobic methane oxidation in Black Sea sediments: Deep-Sea Research Part I, v. 48, p. 2097–2120.

Joye, S. B., Boetius, A., Orcutt, B. N., Montoya, J. P., Schulz, H. N., Erickson, M. J., and Lugo, S. K., 2004, The anaerobic oxidation of methane and sulfate reduction in sediments from Gulf of Mexico cold seeps: Chemical Geology, v. 205, p. 219–238.

Kallmeyer, J., and Boetius, A., 2004, Effects of temperature and pressure on sulfate reduction and anaerobic oxidation of methane in hydrothermal sediments of Guaymas Basin: Applied Environmental Microbiology, v. 70, p. 1231–1233.

Kaprelyants, A. S., Gottschal, J. C., and Kell, D. B., 1993, Dormancy in non-sporulating bacteria: FEMS Microbiology Reviews, v. 104, p. 271–286.

King, G. M., 1984, Utilisation of hydrogen, acetate, and "noncompetitive" substrates by methanogenic bacteria in marine sediments: Geomicrobiology Journal, v. 3, p. 275–306.

Klump, J. V., and Martens, C. S., 1989, The seasonality of nutrient regeneration in an organic-rich coastal sediment: kinetic modeling of changing pore-water nutrient and sulfate distributions: Limnology and Oceanography, v. 34, p. 559–577.

Knittel, K., Boetius, A., Lemke, A., Eilers, H., Lochte, K., Pfannkuche, O., Linke, P., and Amann, R., 2003, Activity, distribution, and diversity of sulfate reducers and other bacteria in sediments above gas hydrate (Cascadia margin, Oregon): Geomicrobiology Journal, v. 20, p. 269–294.

Knoblauch, C., and Jørgensen, B. B., 1999, Effect of growth on sulphate reduction, growth rate and growth yield in five psychrophilic sulphate-reducing bacteria from Arctic sediments: Environmental Microbiology, v. 1, p. 457–467.

Knoblauch, C., Jørgensen, B. B., and Harder, J., 1999, Community size and metabolic rates of psychrophilic sulfate-reducing bacteria in Arctic marine sediments: Applied Environmental Microbiology, v. 65, p. 4230–4233.

Koretsky, C. M., Moore, C. M., Lowe, K. L., Meile, C., DiChristina, T. J., and Van Cappellen, P., 2003, Seasonal oscillation of microbial iron and sulfate reduction in saltmarsh sediments (Sapelo Island, GA, USA): Biogeochemistry, v. 64, p. 179–203.

Koretsky, C. M., Van Cappellen, P., DiChristina, T. J., Kostka, J. E., Lowe, K. L., Moore, C. M., Roychoudhury. A. N., and Viollier, E., 2005, Salt marsh pore water geochemistry does not correlate with microbial community structure: Estuarine Coastal and Shelf Science, v. 62, p. 233–251.

Kotsyurbenko, O. R., Glagolev, M. V., Nozhevnikova, A. N., and Conrad, R., 2001, Competition between homoacetogenic bacteria and methanogenic archaea for hydrogen at low temperature: FEMS Microbiology Ecology, v. 38, p. 153–159.

Kristjansson, J. K., Schönheit, P., and Thauer, R. K., 1982, Different Ks values for hydrogen of methanogenic bacteria and sulfate reducing bacteria: An explanation for the apparent inhibition of methanogenesis by sulfate: Archives of Microbiology, v. 131, p. 278–282.

Krüger, M., Meyerdierks, A., Glöckner, F. O., Amann, R., Widdel, F., Kube, M., Reinhardt, R., Kahnt, J., Böcherm R., Thauer, R. K., and Shima, S., 2003, A conspicuous nickel protein in microbial mats that oxidize methane anaerobically: Nature, v. 426, p. 878–881.

Kvenvolden, K. A., Ginsburg, G., and Soloviev, V., 1993, Worldwide distribution of subaquatic gas hydrates: Geo-Marine Letters, v. 13, p. 32–40.

Lee, M. J., and Zinder, S. H., 1988, Isolation and characterization of a thermophilic bacterium which oxidizes acetate in syntrophic association with a methanogen and which grows acetogenically on H_2-CO_2: Applied Environmental Microbiology, v. 54, p. 124–129.

Lokshina, L. Y., and Vavilin, V. A., 1999, Kinetic analysis of the key stages of low temperature methanogenesis: Ecological Modelling, v. 117, p. 285–303.

Lovley, D. R., and Chapelle, F. H., 1995, A modeling approach to elucidating the distribution and rates of microbially catalyzed redox reactions in anoxic groundwater, *in* Koch, A. L., Robinson, J. A., and Milliken, G. A., editors, Mathematical modeling in microbial ecology: New York, Chapman and Hall, p. 196–209.

Lovley, D. R., and Goodwin, S., 1988, Hydrogen concentrations as an indicator of the predominant terminal electron-accepting reactions in aquatic sediments: Geochimica et Cosmochimica Acta, v. 52, p. 2993–3003.

Lovley, D. R., and Klug, M. J., 1986, Model for the distribution of sulphate reduction and methanogenesis in freshwater sediments: Geochimica et Cosmochimica Acta, v. 50, p. 11–18.

Lovley, D. R., Dwyer, D. F., and Klug, M. J., 1982, Kinetic analysis of competition between sulphate reducers and methanogens for hydrogen in sediments: Applied Environmental Microbiology, v. 43, p. 1373–1379.

Luff, R., and Wallmann, K., 2003, Fluid flow, methane fluxes, carbonate precipitation and biogeochemical turnover in gas hydrate-bearing sediments at Hydrate Ridge, Cascadia Margin: numerical modeling and mass balances: Geochimica et Cosmochimica Acta, v. 67, p. 3403–3421.

Luff, R., Wallmann, K., and Aloisi, G., 2004, Numerical modeling of carbonate crust formation at cold vent sites: significance for fluid and methane budgets and chemosynthetic biological communities: Earth and Planetary Science Letters, v. 221, p. 337–353.

Luna, G. M., Manini, E., and Danovaro, R., 2002, Large fraction of dead and inactive bacteria in coastal marine sediments: comparison of protocols for determination and ecological significance: Applied Environmental Microbiology, v. 68, p. 3509–3513.

Mackenzie, F. T., 1998, Our changing planet: An introduction to earth system science and global environmental change: New Jersey, Prentice Hall, 486 p.

Martens, C. S., Albert, D. B., and Alperin, M. J., 1998, Biogeochemical processes controlling methane in gassy coastal sediments-Part 1. A model coupling organic matter flux to gas production, oxidation and transport: Continental Shelf Research, v. 18, p. 1741–1770.

——— 1999, Stable isotope tracing of anaerobic methane oxidation in the gassy sediments of Eckernförde Bay, German Baltic Sea: American Journal of Science, v. 299, p. 589–610.

Massumi, A., Najafi, N. M., and Barzegari, H., 2002, Speciation of Cr(VI)/Cr(III) in environmental waters by fluorimetric method using central composite, full and fractional factorial design: Microchemical Journal, v. 72, p. 93–101.

Michaelis, W., Seifert, R., Nauhaus, K., Treude, T., Thiel, V., Blumenberg, M., Knittel, K., Gieseke, A., Peterknecht, K., Pape, T., Boetius, A., Amann, R., Jørgensen, B. B. , Widdel, F., Peckmann, J., Pimenov, N. V., and Gulin, M. B., 2002, Microbial reefs in the Black Sea fueled by anaerobic oxidation of methane: Science, v. 297, p. 1013–1015.

Millero, F. J., and Pierrot, D., 1998, A chemical equilibrium model for natural waters: Aquatic Geochemistry, v. 4, p. 153–199.

Montgomery, D. C., 1997, Design and Analysis of Experiments: New York, Wiley, 704 p.

Morel, F. M. M., and Hering, J. G., 1993, Principles and applications of aquatic chemistry: New York, Wiley, 584 p.

Müller, V., 2003, Energy conservation in acetogenic bacteria: Applied Environmental Microbiology, v. 69, p. 6345–6353.

Nauhaus, K., Boetius, A., Kruger, M., and Widdel, F., 2002, In vitro demonstration of anaerobic oxidation of methane coupled to sulphate reduction in sediment from a marine gas hydrate area: Environmental Microbiology, v. 4, p. 296–305.

Nauhaus, K., Treude, T., Boetius, A., Krüger, M., and Krüger, M., 2005, Environmental regulation of the anaerobic oxidation of methane: a comparison of ANME-I and ANME-II communities: Environmental Microbiology, v. 7, p. 98–106.

Niewöhner, C., Hensen, C., Kasten, S., Zabel, M., and Schulz, H. D., 1998, Deep sulfate reduction completely mediated by anaerobic methane oxidation in sediments of the upwelling area off Namibia: Geochimica et Cosmochimica Acta, v. 62, p. 455–464.

Novitsky, J. A., 1987, Microbial growth rates and biomass production in a marine sediment: evidence for a very active but mostly nongrowing community: Applied Environmental Microbiology, v. 53, p. 2368–2372.

Nüsslein, B., Chin, K. J., Eckert, W., and Conrad, R., 2001, Evidence for anaerobic syntrophic acetate oxidation during methane production in the profundal sediment of subtropical Lake Kinneret (Israel): Environmental Microbiology, v. 3, p. 460–470.

Oremland, R. S., and Polcin, S., 1982, Methanogenesis and sulfate reduction: Competitive and noncompetitive substrates in estuarine sediments: Applied Environmental Microbiology, v. 44, p. 1270–1276.

Orphan, V. J., House, C. H., Hinrichs, K. U., McKeegan, K. D., and DeLong, E. F., 2001, Methane-consuming archaea revealed by directly coupled isotopic and phylogenetic analysis: Science, v. 293, p. 484–487.

——— 2002, Multiple archaeal groups mediate methane oxidation in anoxic cold seep sediments: Proceedings of the National Academy of Sciences of the United States of America, v. 99, p. 7663–7668.

Oude Elferink, S. J. W. H., Visser, A., Hulshoff Pol, L. W., and Stams, A. J. M., 1994, Sulfate reduction in methanogenic bioreactors: FEMS Microbiology Reviews, v. 15, p. 119–136.

Pancost, R. D., Damste, J. S. S., De Lint, S., van der Maarel., M. J. E. C., Gottschal, J. C., and The MEDINAUT Shipboard Scientific Party, 2000, Biomarker evidence for widespread anaerobic methane oxidation in Mediterranean sediments by a consortium of methanogenic archaea and bacteria: Applied Environmental Microbiology, v. 66, p. 1126–1132.

Pavlostathis, S. G., and Giraldo-Gomez, E., 1991, Kinetics of anaerobic treatment: Water Science and Technology, v. 24, p. 35–59.

Pirt, S. J., 1965, The maintenance energy of bacteria in growing cultures: Proceedings of the Royal Society of London, v. 163B, p. 224–231.

Poremba, K., and Hoppe, H. G., 1995, Spatial variation of benthic microbial production and hydrolytic enzymatic activity down the continental slope of the Celtic Sea: Marine Ecology Progress Series, v. 118, p. 237–245.

Rabus, R., Hansen, T., and Widdel, F., 2004, Dissimilatory sulfate- and sulfur-reducing prokaryotes, *in* Dworkin, M., and others, editors, The prokaryotes: an evolving electronic resource for the microbiological community, release 3.16: New York, Springer-Verlag, http://link.springer-ny.com/link/service/books/10125

Ravenschlag, H., Sahm, K., Knoblauch, C., Jørgensen, B. B., and Amann, R., 2000, Community Structure, Cellular rRNA Content, and Activity of Sulfate-Reducing Bacteria in Marine Arctic Sediments: Applied and Environmental Microbiology, v. 66, p. 3592–3602.

Reeburgh, W. S., 1976, methane consumption in Cariaco Trench waters and sediments: Earth and Planetary Science Letters, v. 28, p. 337–344.

——— 1980, Anaerobic methane oxidation: rate depth distributions in Skan Bay sediments: Earth and Planetary Science Letters, v. 47, p. 345–352.

——— 1996, "Soft spots" in the global methane budget, *in* Lidstrom, M. E., and Tabita, F. R., editors, Microbial growth on C1 compounds: Dordrecht, Kluwer, p. 334–342.

Rittmann, B. E., and McCarty, P. L., 2001, Environmental biotechnology: Principles and applications: New York, McGraw-Hill Book Company, 768 p.

Rittmann, B. E. and VanBriesen, J. M., 1996, Microbiological processes in reactive modeling, *in* Lichtner, P. C., Steefel, C. I., and Oelkers, E. H., editors, Reactive transport in porous media: Mineralogical Society of America Reviews in Mineralogy, v. 34, p. 311–334.

Robinson, J. A., and Tiedje, J. M., 1984, Competition between sulfate-reducing and methanogenic bacteria for H2 under resting and growing conditions: Archives of Microbiology, v. 137, p. 26–32.

Rothfuss, F., and Conrad, R., 1993, Thermodynamics of methanogenic intermediary metabolism in littoral sediment of Lake Constance: FEMS Microbiology Ecology, v. 12, p. 265–276.

Sahoo, N. R., Pandalai, H. S., and Subramanyam, A., 2000, Secondary geochemical dispersion in the Precambrian auriferous Hutti–Maski schist belt, Raichur district, Karnataka, India. Part II. Application of factorial design in the analysis of secondary dispersion of As: Journal of Geochemical Exploration, v. 71, p. 291–303.

Sansone, F. J., and Martens, C. S., 1982, Volatile fatty acid cycling in organic-rich marine sediments: Geochimica et Cosmochimica Acta, v. 46, p. 1575–1589.

Santegoeds, C. M., Damgaard, L. R., Hesselink, C., Zopfi, J., Lens, P., Muyzer, G., and De Beer, D., 1999, Distribution of sulfate-reducing and methanogenic bacteria in anaerobic aggregates determined by microsensor and molecular analyses: Applied Environmental Microbiology, v. 65, p. 4618–4629.

Schäfer, D., Schäfer, W., and Kinzelbach, W., 1998, Simulation of reactive processes related to biodegradation in aquifers: 1. Structure of the three-dimensional reactive transport model: Journal of Contaminant Hydrology, v. 31, p. 167–186.

Schink, B., 1997, Energetics of syntrophic cooperation in methanogenic degradation: Microbiology and Molecular Biology Reviews, v. 61, p. 262–280.

Schippers, A., Neretin, L. N., Kallmeyer, J., Ferdelman, T. G., Cragg, B. A., Parkes, R. J., and Jørgensen, B. B., 2005, Prokaryotic cells of the deep sub-seafloor biosphere identified as living bacteria: Nature, v. 433, p. 861–864.

Schönheit, P., Kristjansson, J. K., and Thauer, R. K., 1982, Kinetic mechanism for the ability of sulphate reducers to out-compete methanogens for acetate: Archives of Microbiology, v. 132, p. 285–288.

Schulz, S., and Conrad, R., 1996, Influence of temperature on pathways to methane production in the permanently cold profundal sediment of Lake Constance: FEMS Microbiology Ecology, v. 20, p. 1–14.
Segers, R., and Kengen, S. W. M., 1998, Methane production as a function of anaerobic carbon mineralization: A process model: Soil Biology and Biochemistry, v. 30, p. 1107–1117.
Senior, E., Lindstrom, B., Banat, I. M., and Nedwell, D. B., 1982, Sulfate reduction and methanogenesis in the sediment of a saltmarsh on the east coast of the United Kingdom: Applied Environmental Microbiology, v. 43, p. 987–996.
Simpson, P. G., and Whitman, W. B., 1993, Anabolic pathways in methanogens, *in* Ferry, J. G., editor, Methanogenesis: Ecology, physiology, biochemistry and genetics: London, Chapman and Hall, p. 445–472.
Sørensen, K. B., Finster, K., and Ramsing, N. B., 2001, Thermodynamic and kinetic requirements in anaerobic methane oxidizing consortia exclude hydrogen, acetate, and methanol as possible electron shuttles: Microbial Ecology, v. 42, p. 1–10.
Starzec, P., and Andersson, J., 2002, Application of two-level factorial design to sensitivity analysis of keyblock statistics from fracture geometry: International Journal of Rock Mechanics and Mineral Science, v. 39, p. 243–255.
Talin, F., Tolla, C., Rabouille, C., and Poggiale, J. C., 2003, Relations between bacterial biomass and carbon cycle in marine sediments: an early diagenetic model: Acta Biotheoretica, v. 51, p. 295–315.
Thauer, R. K., Jungermann, K., and Decker, K., 1977, Energy conservation in chemotrophic anaerobic bacteria: Bacteriological Reviews, v. 41, p. 100–180.
Thomsen, T. R., Finster, K., and Ramsing, N. B., 2001, Biogeochemical and molecular signatures of anaerobic methane oxidation in a marine sediment: Applied Environmental Microbiology, v. 67, p. 1646–1656.
Thornton, S. F., Quigley, S., Spence, M. J., Banwart, S. A., Bottrell, S., and Lerner, D. N., 2001, Processes controlling the distribution and natural attenuation of dissolved phenolic compounds in a deep sandstone aquifer: Journal of Contaminant Hydrology, v. 52, p. 233–267.
Thullner, M., Van Cappellen, P., and Regnier, P., 2005, Modeling the impact of microbial activity on redox dynamics in porous media: Geochimica et Cosmochimica Acta, v. 69, p. 5005–5119.
Tijhuis, L., van Loosdrecht, M. C. M., and Heijnen, J. J., 1993, A thermodynamically based correlation for maintenance Gibbs energy requirements in aerobic and anaerobic chemotrophic growth: Biotechnology and Bioengineering, v. 42, p. 509–519.
Treude, T., Boetius, A., Knittel, K., Wallmann, K., and Jørgensen, B. B., 2003, Anaerobic oxidation of methane above gas hydrates at Hydrate Ridge, NE Pacific Ocean: Marine Ecology Progress Series, v. 264, p. 1–14.
Treude, T., Krüger, M., Boetius, A., and Jørgensen, B. B., 2005, Environmental control on anaerobic oxidation of methane in the gassy sediments of Eckernförde Bay (German Baltic): Limnology Oceanography, v. 50, p. 1771–1786.
van Bodegom, P. M., and Scholten, J. C. M., 2001, Microbial processes of CH_4 production in a rice paddy soil: Model and experimental validation: Geochimica et Cosmochimica Acta, v. 65, p. 2055–2066.
VanBriesen, J. M., 2002, Evaluation of methods to predict bacterial yield using thermodynamics: Biodegradation, v. 13, p. 171–190.
Van Cappellen, P., and Gaillard, J. F., 1996, Biogeochemical dynamics in aquatic sediments, *in* Lichtner, P. C., Steefel, C. I., and Oelkers, E. H., editors, Reactive transport in porous media: Mineralogical Society of America Reviews in Mineralogy, v. 34, p. 335–376.
Van Cappellen, P., and Wang, Y., 1996, Cycling of iron and manganese in surface sediments: a general theory for the coupled transport and reaction of carbon, oxygen, nitrogen, sulfur, iron, and manganese: American Journal of Science, v. 296, p. 197–243.
Vavilin, V. A., Lokshina, L. Ya., Rytov, S. V., Kotsyurbenko, O. R., Nozhevnikova, A. N., and Parshina, S. N., 1997, Modelling methanogenesis during anaerobic conversion of complex organic matter at low temperatures: Water Science and Technology, v. 36, p. 531–538.
Visser, A., Beeksma, I., van der Zee, F., Stams, A. J. M., and Lettinga, G., 1993, Anaerobic degradation of volatile fatty acids at different sulphate concentrations: Applied Microbiology and Biotechnology, v. 40, p. 549–556.
Watson, I. A., Oswald, S. E., Mayer, K. U., Wu, Y., and Banwart, S. A., 2003, Modeling kinetic processes controlling hydrogen and acetate concentrations in an aquifer-derived microcosm: Environmental Science and Technology, v. 37, p. 3910–3919.
Wellsbury, P., Herbert, R. A., and Parkes, R. J., 1996, Bacterial activity and production in near-surface estuarine and freshwater sediments: FEMS Microbiology Ecology, v. 19, p. 203–214.
Westermann, P., Ahring, B. K., and Mah, R. A., 1989, Temperature compensation in *Methanosarcina barkeri* by modulation of hydrogen and acetate affinity: Applied Environmental Microbiology, v. 55, p. 1262–1266.
Weston, N. B., and Joye, S. B., 2005, Temperature-driven decoupling of key phases of organic matter degradation in marine sediments: Proceedings of the National Academy of Sciences of the United States of America, v. 102, p. 17036–17040.
Westrich, J. T., and Berner, R. A., 1984, The role of sedimentary organic matter in bacterial sulfate reduction: the G-model tested: Limnology and Oceanography, v. 29, p. 236–249.
——— 1988, The effect of temperature on rates of sulfate reduction in marine sediments: Geomicrobiology Journal, v. 6, p. 99–117.
Whiticar, M. J., Faber, E., and Schoell, M., 1986, Biogenic methane formation in marine and freshwater environments: CO_2 reduction *vs.* acetate fermentation—Isotope evidence: Geochimica et Cosmochimica Acta, v. 50, p. 693–709.
Whitman, W. B., Coleman, D. C., and Wiebe, W. J., 1998, Prokaryotes: The unseen majority: Proceedings of the National Academy of Sciences of the United States of America, v. 95, p. 6578–6583.

Whitman, W. B., Bowen, T. L., and Boone, D. R., 2004, The methanogenic bacteria, *in* Dworkin, M., and others, editors, The prokaryotes: an evolving electronic resource for the microbiological community, release 3.16: New York, Springer-Verlag, http://link.springer-ny.com/link/service/books/10125/.

Widdel, F., 1988, Microbiology and ecology of sulfate- and sulfur-reducing bacteria, *in* Zehnder, A. J. B., editor, Biology of anaerobic microorganisms: New York, John Wiley and Sons, p. 469–585.

Winfrey, M. R., and Ward, D. M., 1983, Substrates for sulfate reduction and methane production in intertidal sediments: Applied Environmental Microbiology, v. 45, p. 193–199.

Yamamoto, S., Alcauskas, J. B., and Crozier, T. E., 1976, Solubility of methane in distilled water and seawater: Journal of Chemical and Engineering Data, v. 21, p. 78–80.

Yuan, Z., and VanBriesen, J. M., 2002, Yield prediction and stoichiometry of multi-step biodegradation reactions involving oxygenation: Biotechnology and Bioengineering, v. 80, p. 100–113.

Zehnder, A. J. B., and Stumm, W., 1988, Geochemistry and biogeochemistry of anaerobic habitats, *in* Zehnder, A. J. B., editor, Biology of anaerobic microorganisms: New York, John Wiley and Sons, p. 1–38.

Zinder, S. H., 1993, Physiological ecology of methanogens, *in* Ferry, J. G., editor, Methanogenesis: Ecology, physiology, biochemistry and genetics: London, Chapman and Hall, p. 128–206.

——— 1994, Syntrophic acetate oxidation and reversible acetogenesis, *in* Drake, H. L., editor, Acetogenesis: London, Chapman and Hall, p. 386–415.

Zinder, S. H., and Koch, M., 1984, Non-aceticlastic methanogenesis from acetate: Acetate oxidation by a thermophilic syntrophic coculture: Archives of Microbiology, v. 138, p. 263–272.